Radio Frequency Power Amplifiers Adapted for Low Field Magnetic Resonance Imaging

A thesis submitted to the

College of Graduate and Postdoctoral Studies

in partial fulfillment of the requirements

for the degree of Master of Science

in the Division of Biomedical Engineering

University of Saskatchewan

Saskatoon

By

Faezeh Ebadollahi Somee

Permission to Use

In presenting this thesis in partial fulfillment of the requirements for a Postgraduate degree from the University of Saskatchewan, I agree that the Libraries of this University may make it freely available for inspection. I further agree that permission for copying of this thesis in any manner, in whole or in part, for scholarly purposes may be granted by the professor or professors who supervised my thesis work or, in their absence, by the Head of the Department or the Dean of the College in which my thesis work was done. It is understood that any copying or publication or use of this thesis or parts thereof for financial gain shall not be allowed without my written permission. It is also understood that due recognition shall be given to me and to the University of Saskatchewan in any scholarly use which may be made of any material in my thesis.

Disclaimer

Reference in this thesis to any specific commercial products, process, or service by trade name, trademark, manufacturer, or otherwise, does not constitute or imply its endorsement, recommendation, or favoring by the University of Saskatchewan. The views and opinions of the author expressed herein do not state or reflect those of the University of Saskatchewan, and shall not be used for advertising or product endorsement purposes.

Requests for permission to copy or to make other uses of materials in this thesis in whole or part should be addressed to:

Head of the Division of Biomedical Engineering

Room 2B60 Engineering Building

University of Saskatchewan

57 Campus Drive

Saskatoon, Saskatchewan

Canada

S7N 5A9

OR

Dean

College of Graduate and Postdoctoral Studies

University of Saskatchewan

116 Thorvaldson Building, 110 Science Place

Saskatoon, Saskatchewan S7N 5C9 Canada

Abstract

Magnetic Resonance Imaging (MRI) is a reliable and established minimally invasive imaging technique that can provide diagnostically relevant information about the internal structures of the human body. While the basic design of the new MRI scanners is not much different from when they were first designed a few decades ago, finding new ways to modify these big, power-hungry, expensive and complex systems is becoming more and more essential. One of the ways of removing the restrictions that conventional MRI systems have is making them low field. This leads to lighter, smaller, simpler and less expensive MRI scanners that can potentially become portable. Once they are portable, MRI scanners can have various applications ranging from being used in emergency and operating rooms to being taken to remote areas and even outer space. The Space MRI Lab at the University of Saskatchewan focuses on building prototypes of portable MRIs for monitoring astronaut health by using TRansmit Array Spatial Encoding (TRASE). TRASE is an innovative MRI method that operates without relying on noisy, heavy and complex gradient coils. In TRASE, the spatial encoding happens based on the phase gradients of the transmit radio frequency (RF) magnetic field.

TRASE-based MRI scanners have specific requirements. One of those requirements is RF power amplifiers (RFPAs) with high-power RF output, high duty cycle and fast switching times. These characteristics are important for achieving maximal TRASE MRI resolution. However, since no commercially available RFPA with these specifications exists, it was necessary to build RFPAs customized for TRASE applications. A class A/B Ham radio power amplifier design was modified to be more compatible with TRASE-based MRIs. As part of

this thesis, two of these RFPAs were constructed at the University of Saskatchewan Space MRI Lab. The RFPAs were assembled to be used with the Merlin MRI, an ankle-sized portable MRI tested in zero-gravity which uses TRASE. Fortunately, both of the RFPAs showed expected results at the testing stage and have since been integrated with the Merlin MRI. Details of the assembly work are presented in this thesis.

Acknowledgements

I have been so lucky that even by starting to think about writing this section my mind gets filled by the countless names without whose support and encouragement I would never have been able to come as far as finishing my journey as a M.Sc. student. I would like to seize this opportunity to express my genuine gratitude to all who have helped me along the way and thank them for being present for me whenever I needed them.

First of all, I want to thank my supervisors Dr. Gordon E. Sarty and Dr. Kathryn McWilliams for all the kindness, patience, guidance and encouragement they have shown me in the past few years. I would not have had the chance to enter this amazing world of wonders if it was not for them. Working at the Space MRI Lab has been one of the most exciting experiences of my life, it does not mean that it has not been challenging, but if it was not for the opportunity to face such challenges, I never would have pushed myself and grown, and for that, I am forever grateful to Dr. Sarty. I was fortunate enough to have supervisors who not only are outstanding researchers and academics, but also they are wonderful human beings who have taught me a lot about how to live by just being who they are. I am grateful for all they have taught me, all the priceless advice they have given me and all the compassion they have shown me throughout my time as their student.

I would also like to thank both of my advisory committee members, Dr. Jonathan C. Sharp for his invaluable advice and suggestions during the committee meetings and Dr. Michael P. Bradley for his sincere support and also for granting me access to the Plasma Physics lab in the Physics department at the University of Saskatchewan and making it possible for me to use the equipment I needed while I was building electronic parts.

I want to express my gratitude towards Farnaz Zohourparvaz, Dr. Pallavi Bohidar and Dr. Hammed Ejalonibu, who initially were amazing people I was working with in the same lab and later on turned into incredible friends.

I want to thank Dr. Aaron Purchase for all his help and advice through multiple emails and meetings during the time I was working on the construction of amplifiers. His genuine willingness to help made the process a lot easier.

I acknowledge and appreciate the funding provided by Natural Sciences and Engineering Research Council of Canada (NSERC) through the Collaborative Research and Training Experience (CREATE) program guided by Dr. McWilliams and the funding provided to Dr. Sarty by the Canadian Space Agency (CSA) FAST grant that supported the work done during my degree and in this thesis.

Last but not least, I would like to express my deepest love and gratitude to my parents, my brother and my amazing friends who were always with me every step of the way.

I dedicate this thesis to my mother, Masoumeh Minaei. Without her boundless love, ever-present support and countless sacrifices, I do not know who I would be in this world.

Contents

List of Tables

List of Figures

List of Abbreviations

MRI	Magnetic Resonance Imaging
NMR	Nuclear Magnetic Resonance
RF	Radio Frequency
POC	Point Of Care
TRASE	TRansmit Array Spatial Encoding
NRC	National Research Council of Canada
RFPA	Radio Frequency Power Amplifier
SNR	Signal to Noise Ratio
LNA	Low Noise Amplifier
SDR	Software Defined Ratio
T/R	Transmit/Receive
ISS	International Space Station
FAST	Flights and Fieldwork for the Advancement of Science and Technology Funding Initiative
MOSFET	Metal Oxide Semiconductor Field-Effect Transistor
FOV	Field Of View
BS	Bloch-Siegert
FPGA	Field Programmable Gate Array
VLF	Very Low Field
ULF	Ultra Low Field

NdFeB	Neodymium-Iron-Boron
PCB	Printed Circuit Boards
rSEM	rotating Spatial Encoding Magnetic field
PCB	Printed Circuit Boards
TNMR	Tecmag Apollo
SAR	Specific Absorption Rate
pMRI	portable Magnetic Resonance Imaging
GE	General Electric
iMRI	intra operative Magnetic Resonance Imaging
LED	Light-Emitting Diode
1D	One-Dimensional
2D	Two-Dimensional
3D	Three-Dimensional
FDA	US Food and Drug Administration
EMI	Electromagnetic Interference
OAI	Open-Access Imager
ADC	Apparent Diffusion Contrast
CSA	Canadian Space Agency
SMACS	Standard Merlin Awesome Coordinate System
AD2	Analog Discovery 2 (a USB oscilloscope and logic analyzer)
IC	Integrated Circuit
AFP	Adiabatic Full Passage

USASK	University of Saskatchewan
U of A	University of Alberta
BOM	Bill Of Material
CMCD	Current Mode Class D
PSU	Power Supply Unit
FET	Field-Effect Transistor
BJT	Bipolar Junction Transistor

1 Introduction

1.1 Magnetic Resonance Imaging for Astronauts

Magnetic Resonance Imaging (MRI) is a medical imaging technique that uses Nuclear Magnetic Resonance (NMR) to acquire images of anatomical structures by utilizing a magnetic field and Radio Frequency (RF) signals. Although traditional MRI scanners are more complex than most of the other imaging devices, they are significant in the medical imaging world since they can selectively image various tissue characteristics that provide diagnostically valuable information [1]. However, traditional MRIs are big and expensive, they require huge spaces, need shielding and are not always easily accessible to everyone and at all places. Fortunately, in the recent years there have been more and more efforts towards achieving portability for MRI systems. One way to do this is by removing gradient coils in MRI scanners. B_0 gradient coils are very heavy and noisy parts of MRI systems which are also responsible for creating eddy currents inside patients' bodies and other nearby conductive materials. There are various ways to make gradient-free MRIs. The main difference between traditional MRIs, and the gradient-free versions, is that the former uses B_0-encoding while the latter uses B_1-encoding. In gradient-free MRI, spatial information is encoded into the NMR signal by altering the transmitted RF field. This makes MRIs considerably simpler, cheaper and lighter, and therefore portable, allowing their usage to be expanded [2].

1.1.1 MRI For Space

An important benefit portable MRI systems can provide is to facilitate medical imaging in space which is the focus of the Space MRI Lab at the University of Saskatchewan. Microgravity causes astronauts to lose bone and muscle mass during long space missions. This is a major health issue, and hence ways of monitoring the bone and muscle health for astronauts are of utmost importance. Although the bone and muscle mass are assessed before and after space missions, portable MRIs can make a big difference since they provide the opportunity to monitor how bone and muscle density change throughout a mission. [3, 4]

There are various ways of building portable MRIs. The technique that is being used at the Space MRI Lab is called TRansmit Array Spatial Encoding (TRASE). In TRASE, image information is encoded by the manipulation of Radio frequency (RF) transmission [2]. The Space MRI Lab is working on building low-field, light-weight, low-cost, portable prototypes of MRI scanners for astronaut health monitoring.

1.1.2 General Need For Portable MRIs

The weight of traditional MRIs can exceed five tons and since they create strong magnetic fields, they require electrically shielded rooms to eliminate noise sources. Removing gradient coils makes drastic changes, which can help to make MRI scanners more accessible [5]. Right now, many people living in remote areas, in countries with high population densities or limited access to medical facilities do not have the opportunity to benefit from MRIs' privileges. Portable MRIs can provide different advantages such as limiting the need for the emergency transportation of patients.

1.2 Thesis Objectives and Overview

This thesis consists of two parts. The first part is a review of already-existing portable MRIs and the second part includes research on RF power amplifiers. The objective of this thesis work was to review the new portable, low-field MRIs and to construct a radio frequency power amplifier needed for the development of low-field MRIs at the Space MRI Lab. Using TRASE requires specific RF power amplifiers, which is the electronic component that was constructed as part of this thesis. The generation of high-power RF pulses is needed in order to collect sufficient k-space data points to form an image. However, commercial RF power amplifiers could not provide this since they could not generate high-power RF output, high duty cycle and fast switching times all at the same time, therefore, a specific design was chosen and assembled.

This thesis consists of five main chapters. The second chapter includes a review of the existing portable MRI technology. Notable designs of portable MRIs that have been built all over the world are included in this chapter. Chapter 3, describes the basics of MRI and gives a background on how MRI works. Additionally, it explains how traditional MRI scanners are different from the new portable ones, and also what it takes to make an MRI scanner portable. Gradient-free methods for magnetic resonance imaging, including TRASE, are briefly discussed in this chapter. Comparisons are also made between TRASE and conventional MRI scanners. Chapter 4, begins with a discussion of amplifier theory. Amplifier characteristics and classes are described in this chapter and TRASE requirements for RF power amplifiers are discussed. Details about the amplifiers constructed as part of this thesis is covered, including the work done assembling and testing a specific non-commercial type

of RF power amplifier to make it compatible with TRASE prototypes of MRI, designed for space applications. The last chapter of this thesis includes the conclusions.

2 Review of Existing Portable MRI Technology

Magnetic Resonance Imaging (MRI) is a non-invasive tool for medical imaging that has been around for a few decades. The definition of low-field MRI refers to any magnetic field strength between 0.001 to 0.2 T, whereas high-field MRI scales refer to the main magnetic field strength being 1.5 T or above, mid-field MRI in the range of 0.2 - 1 T, very-low-field (VLF) around some mT and ultra-low-field (ULF) is in the μT range. For almost 30 years, high-field MRI has been the main method of MRI due to signal-to-noise ratio (SNR) limitations at lower magnetic field strengths. [6, 7]. However, with the more advanced technology now available and the increasing demand for more accessible, less expensive and lighter MRI scanners, low-field MRI is being widely reconsidered. Once low-field MRI scanners that can produce diagnostically relevant images become commercially available, they will cause a huge change in point-of-care (POC) MRI applications. Many people who live in remote areas and less developed countries could greatly benefit from this. As mentioned before, this would include accessibility to MRI scanners in space for monitoring astronauts, especially their muscle and bone health. In this chapter, some of the prototypes of portable MRIs that have been built around the world are reviewed with some of their major characteristics. Figure 2.1 shows a generic block diagram of an MRI scanner. It contains all the necessary parts that are used in

a traditional MRI system including the RF amplifier, which is the part that was assembled as part of this thesis and is discussed thoroughly later in this document.

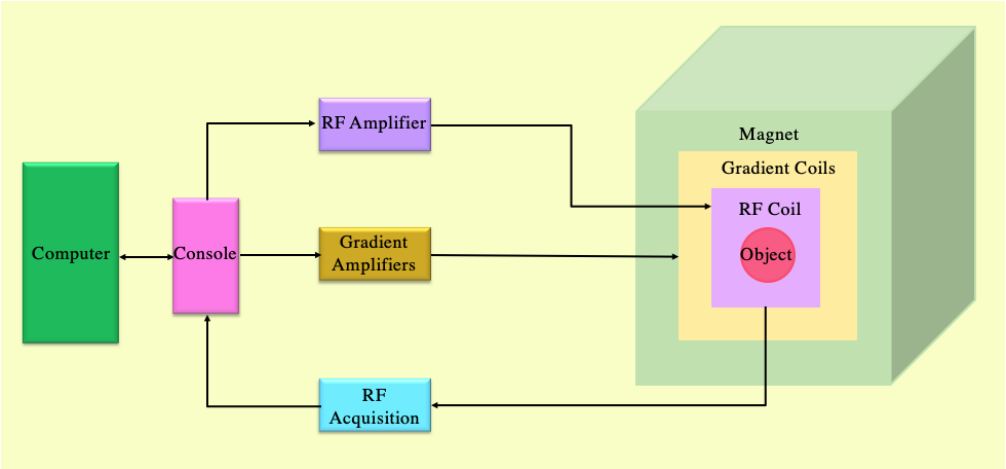

Figure 2.1: Generic block diagram of an MRI scanner.

2.1 Hyperfine's Swoop Portable MRI System

Hyperfine's Swoop MRI is a head-sized, low-field MRI that weighs 630 kg, uses a permanent B_0 magnet with 0.064 T magnetic field strength that measures 140 cm in height and 86 cm in width. This device was developed for POC applications such as emergency rooms and intensive care units. Hyperfine uses Advanced AI applications which is a deep learning image analysis software that measures brain structure and pathology. It utilizes a biplanar, unshielded gradient system with gradient coils for the x, y and z directions. Therefore, it can provide images in any 3D orientation similar to traditional MRI systems. The peak amplitudes of the gradients is 25 mT/m in x and y directions and 26 mT/m in the z direction. To facilitate the movement of this device, motorized wheels are included in its design and it can be controlled using wireless tablets such as an Apple's iPad to deliver initial scan results in a minimum time of 30 minutes [8–10].

The Swoop portable MRI (pMRI) system received 510(k) clearance from the US Food and Drug Administration (FDA) in August 2020 for MR Imaging of the brain and head of patients of all ages and is commercially available. This MRI system claims to reduce acquisition costs by 20 times and consume 35 times less power than existing conventional MRI scanners. The Hyperfine MRI device can be positioned at the head of the patient's hospital bed and be used for general brain imaging including headaches, stroke and encephalopathy issues; it can also be used to monitor Covid-19 patients who are at risk of neurological disorders [7–9, 11–13].

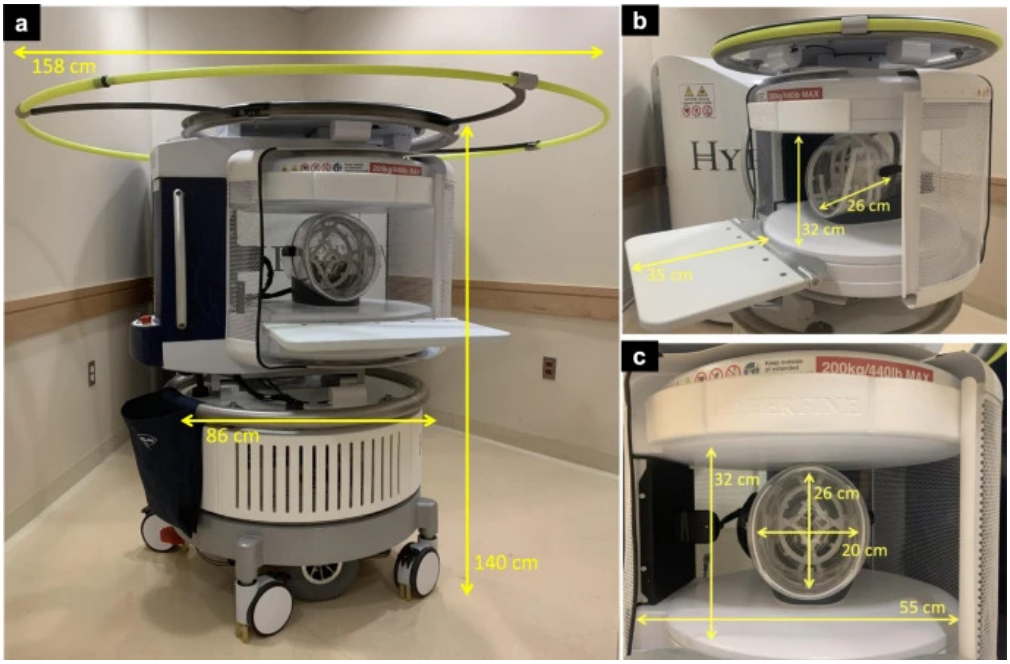

Figure 2.2: Hyperfine's MRI magnet is 140 cm x 86 cm and uses motorized wheels for movement. *Image and caption reproduced from article [14] with Creative Commons CC permission from publisher 'Springer Nature'.*

2.2 The MR Cap

The "MR Cap" is a single-sided MRI system designed by Cooley et al. [15] in 2019 for potential POC imaging of the brain over a 3D volume. The device is in the shape and size

of a standard bicycle helmet (cap-shaped) and when positioned on an adult head, it has a sensitive volume that extends 3 cm beneath the scalp. This under-10-kg pMRI is attached to an adjustable arm which facilitates movement of the sensitive volume to different areas of the brain. The B_0 magnet used in the MR Cap was designed from Neodymium-Boron-Iron (NdFeB) permanent magnets and to maximize the B_0 field strength, it has been built to fit an adult head as closely as possible. The mean B_0 of the constructed version of this pMRI is 0.064 T within the region of interest (ROI) and the measured range of variation across the ROI is 4.40 mT. The constructed magnet weighs 6.3 kg and has a built-in field gradient of about 117 mT/m [15].

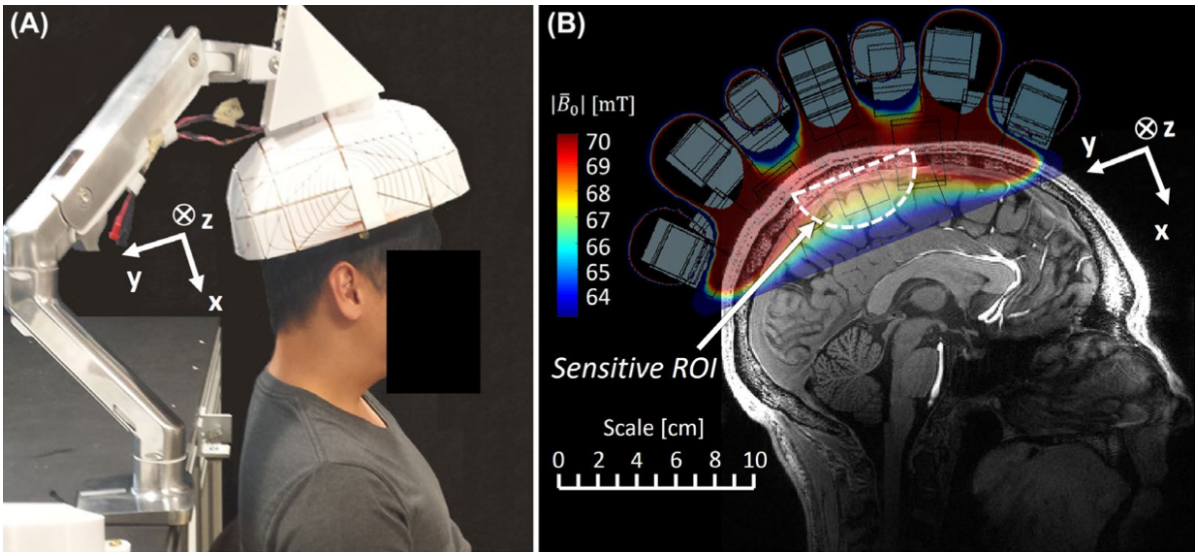

Figure 2.3: a, An illustration of how the "MR Cap" might be positioned and moved about the patient's head. b, Description of a proposed B_0 map with built-in readout encoding gradients. *Image and caption reproduced from article [15] with permission (license number: 5357400816840) from publisher: 'John Wiley and Sons'.*

The MR Cap uses two cap-shaped gradient coils for blipped phase encoding of a spin-echo train along the y- and x- axes. The coils are set on the outside surface of the B_0 magnet to save the inside space for achieving a stronger magnet and to improve gradient linearity

(which reduced the gradient efficiency). The MR Cap also has an T/R RF coil fitting inside the B_0 magnet that has a 157 kHz bandwidth. This RF coil is responsible for optimizing spatial B_1 uniformity within the target ROI and was constructed using four turns of Litz wire and press-fitting them into a 3D-printed polycarbonate former with numerically derived grooves [15].

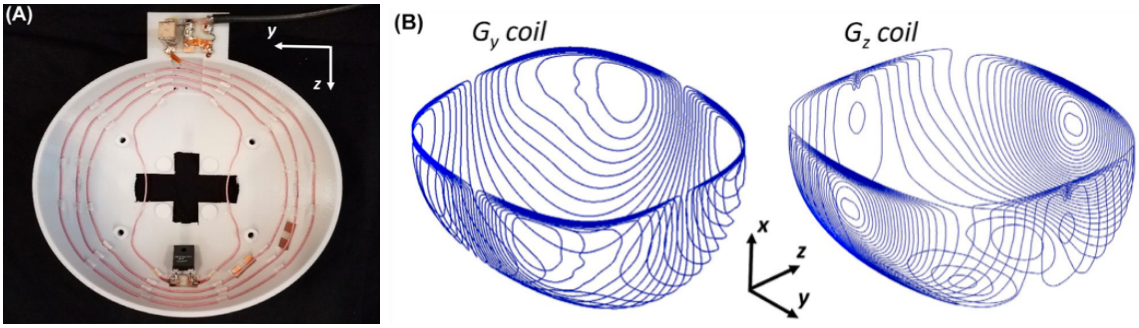

Figure 2.4: a, Volume RF T/R coil constructed using Litz wire. b, Numerical designs for MR Cap's G_y and G_z gradient coils. *Image and caption reproduced from article [15] with permission (license number: 5357400816840) from publisher: 'John Wiley and Sons'.*

To generate RF and gradient waveforms and to record signals in all experiments, the MR Cap team used an Apollo console. Additionally, the RF subsystem used a cross-diode passive T/R switch, wideband pre-amplifier and a 2-kW-rated RFPA. Two homemade current-mode amplifiers capable of driving ±10 A with a voltage of ±15 V were used to drive the gradient coils. A sixth-order Butterworth filter (f_c = 500 kHz) was used to noise filter the gradient drive and all experiments were performed in a shielded environment. Although the MR Cap has been used for experiments and shown reliable data, several practical requirements need to be overcome before it could be used for POC applications (In-vivo imaging in unshielded environments must be tested, temperature-induced shift in B_0 caused by permanent magnet systems needs to be taken care of, replacing high-cost laboratory-grade instruments that were

used during the testing stage with more reasonable ones, etc.) [15].

2.3 Small Car-mounted MRI System for Elbow Imaging in Baseball Injuries

In 2019, a team consisting of the University of Tsukuba students in the department of Applied Physics and researchers from Department of Diagnostic and Interventional Radiology in Japan developed a compact MRI system which can be installed in a minivan. This is a low-field MRI system with a homogeneous 0.2 T permanent magnet that weighs 200 kg and can provide clinically relevant images of elbow injuries. All the MRI setup including the magnet, gradient coils, a home-built RF coil with shielding clothes and the MRI console (80 kg) can easily fit into the vehicle [16, 17].

Figure 2.5: Some images of the Baseball Elbow MRI system, the minivan it was installed in and the elbow images it is able to provide. *Image and caption reproduced from article [16] with permission (license number: 5357410297482) from publisher: 'Elsevier'*

The size of the RF coil used in this project was sufficiently large to allow imaging for

most of the junior baseball players. To electronically shield the subject, conductive shielding clothes were used with the RF shield box and to further reduce the external noise, additional shielding clothes were used while imaging. Each biplanar gradient coil element was constructed using printed circuit boards (PCBs). Then the x, y and z PCB gradients were stacked, wired and fixed firmly, however, no cooling systems or shields were used on gradients. The MRI electronics consisted of a digital transciever, a gradient driver, a +30 dB pre-amplifier, an active T/R switch and an RFPA that were all installed in a 56 cm x 77 cm x 60 cm rack [16]. The team reports that the mean SNR for the in-vehicle measurements was almost the same as the indoor measurements and this value was about 60% of the mean SNR for a commercial MRI scanner.

2.4 Lightweight Gradient-Free MRI for 2D Imaging

In 2015, Cooley et al. [18] built a lightweight (under 100 kg), silent MRI scanner using a rotating cryogen-free, low-field magnet. They used the inhomogeneous field pattern created by a permanent rotating 0.077 T B_0 magnet as a rotating Spatial Encoding Magnetic field (rSEM) to create generalized projections to encode the 2D image. They also added multiple receive channels to disambiguate the encoding field. The rotation of this 45 kg magnet's inhomogeneous field pattern eliminates the need for heavy, switchable, power-hungry gradient coils by replacing their function [17, 18].

In their method, they physically rotate the quadrupolar SEM fields around the object along with the B_0 field and use RF coils to acquire projections of the object with spin-echo train sequences. Their system is also compatible with RF encoding schemes such as TRASE

which can make encoding in the third dimension possible and lead to full 3D encoding [18,19].

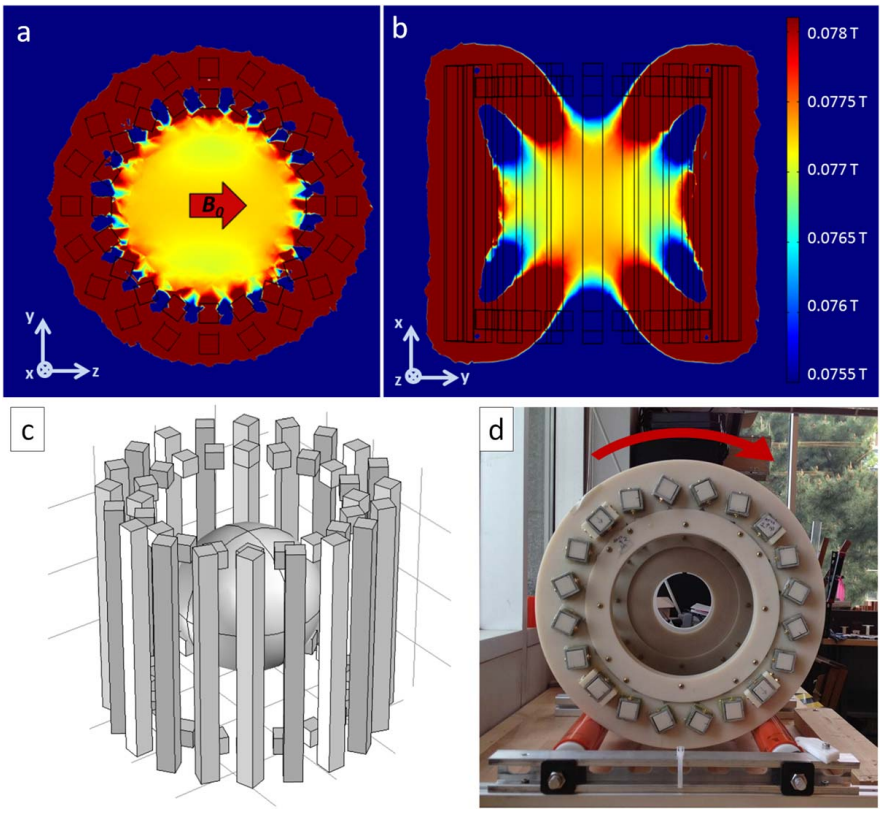

Figure 2.6: a and b: Simulations of the magnetic field in two planes. c: Schematic of arrays of NdFeB magnets and the targeted spherical region which is 18 cm in diameter. d: End-view image of the magnet mounted on rollers. *Image and caption reproduced from article [18] with permission (license number: 1252216-1) from publisher: 'John Wiley and Sons'.*

They use a dipolar Halbach cylinder magnet to produce a rotating B_0 field which is approximately uniform and allows for maximum average field for the highest SNR. The magnet's average field in the 16-cm Field Of View (FOV) is 77.3 mT and responds to a 3.29 MHz proton Larmor frequency. Also, seven NMR field coils are used for mapping the static magnetic field. The coils are held stationary while the magnet is rotated around them. A Tecmag Apollo console with TNMR software that has one transmit channel, three gradient channels (used for other purposes since they are not needed for gradient coils) and one receive

channel are used. A stepper motor controlled by the G_z gradient output of the MRI console is also used for magnet rotation. The rotation is incorporated into the pulse sequence to increase the precision. A RelComm Technologies relay along with the G_x gradient output and Arduino UNO board are needed to switch between receive coils. A copper mesh Faraday cage is also required for enclosing the magnet assembly to reduce RF interference. Shimming was done to decrease field variation with the addition of small shim magnets [18].

Although the B_0 field of the magnet is oriented along the bore of the magnet in conventional MRIs, it is oriented radially in the Halbach magnet. This makes a solenoid coil a better fit than a birdcage coil for RF excitation. The magnet gets rotated around the sample to acquire data in discrete steps. The Rx coil array has eight 8-cm-diameter loops of wire that encircle the FOV on the surface of a 14-cm-diameter cylinder and the solenoid coil has a 20-cm diameter and a 25-cm length. The coils were also matched to 50Ω impedance low noise pre-amplifiers. Geometric decoupling was done and PIN diode detuning was implemented to prevent coil interaction in the transmit and receiver coils. To improve SNR in a spin-echo train, the encoding can be repeated and averaged. Also, the specific absorption rate (SAR) from the consecutive 180° pulses is negligible due to the low excitation frequency. A 1 KW power amplifier is used to generate short 600 W pulses for broadband excitation [18].

2.5 Compact Hand and Wrist MRI for Skeletal Age Assessment in Children

Terada et al. [20] used a new, dedicated hand MRI system in 2012 with a permanent magnet to examine skeletal age in children. The magnet was C-shaped, made of NdFeB material with

a field strength of 0.3 T and weighed 450 kg. Also, a solenoid RF coil, a gradient coil set and an MRI console were included in the setup, and the RF coil was optimized for imaging a child's hand and wrist [20, 21].

Figure 2.7: Overview of an open, compact MRI scanner used on a volunteer patient. *Image and caption reproduced from article [20] with permission (license number: 5357420828479) from publisher: 'John Wiley and Sons'.*

2.6 3D Brain and Extremity Ultra-Low-Field MRI

O'Reilly et al. from Leiden University Medical Centre in the Netherlands (2020) [22] developed a low-cost, portable, VLF MRI system that uses a permanent magnet Halbach array to produce a magnetic field with 0.050 mT strength for in-vivo MRI. Their setup includes the magnet, custom-built gradient coils and their amplifiers and RF coil and its amplifier. They claim to have built this MRI system with hardware components costing less than 10,000 Euros. Their magnet including all its components weighs about 75 kg, gradient and RF amplifiers each weigh 15 kg, gradient coils are 10 kg and the spectrometer is 5 kg [22].

The Halbach magnet used by O'Reilly's team consists of 23 rings with two layers of N48 neodymium boron iron magnets per ring. An optimization technique was used in the design of the ring diameters to provide the highest B_0 homogeneity. The setup also uses additional shimming. The entire setup was placed inside a Faraday cage made of aluminum sheets to minimize the environmental noise. The solenoid RF coil that was used for the phantom and knee imaging experiments as a transmit/receive coil was 15 cm both in length and in diameter and had 57 windings. To decrease the interaction between the self-resonant modes of the gradient coils and the RF coil, as well as to reduce the noise coupled into the system from the gradient amplifier, a thin copper sheet with a width of 50 μm was inserted inside the gradient coils. For in-vivo imaging, an elliptical solenoid was constructed with a length of 20 cm, width of 18.5 cm and height of 24.5 cm with 40 windings. Also, to reduce the eddy currents induced by switching of the gradients, six 800-pF chip capacitors were set along the seam of the sheet. Each gradient power amplifier (GPA) had been constructed using a push-pull configuration [22].

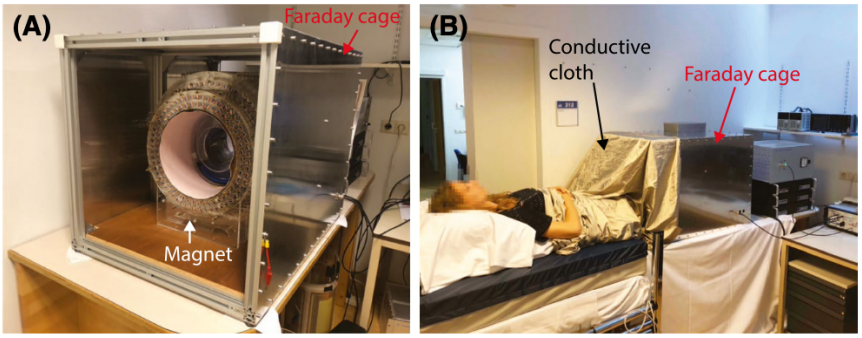

Figure 2.8: A, Shows the magnet setup with the shims and the gradients integrated into the bore of the magnet. The aluminum Faraday cage is used to reduce environmental noise in the setup. B, To reduce the noise coupled into the system through the body a conductive cloth is placed over the subject. *Image and caption reproduced from article [22] with Creative Commons CC permission from publisher 'John Wiley and Sons'.*

2.7 The Applause by MagneVu

An older portable MRI system is The Applause (or MV1000) which was manufactured by MagneVu (Carlsbad, CA), a wrist-sized MRI with a 0.2T, U-shaped, non-uniform, permanent magnet that weighed about 90 kg and utilized a permanent slice-selecting gradient in the B_0 while phase encoding gradients were applied in the selected image plane. The Applause was the first ever MRI scanner to be mounted on wheels and was approved by FDA and used to be distributed by General Electric (GE) Medical Systems. MagneVu went out of business in 2007 [17, 23–26]. This portable MRI used a set of rapidly focused spin echoes to offset the loss of SNR resulting from the diffusion and the non-uniform field. The Applause was an extremity MRI that did not require RF shielding and had applications in foot, wrist and hand imaging [23, 24, 27].

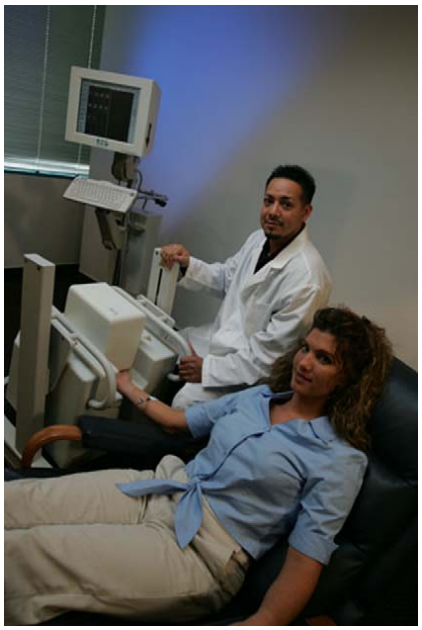

Figure 2.9: The MagneVu extremity scanner being used on a patient. *Image and caption reproduced from article [24] with permission (license number: 5357430976777) from publisher: 'Elsevier'.*

2.8 Medtronic PoleStar iMRI for Neurosurgery

Polestar N20 scanner is a portable low-field (0.15 T) intraoperative MRI (iMRI) system with the StealthStation navigation system for neurosurgery and was designed to be used in an existing conventional operating room in 2007, mainly to assist brain tumour resections. Figure 2.10 shows the main components of the iMRI system. The scanner uses a small 0.15 T permanent magnet and conventional magnetic field gradient coils for spatial encoding. These disk-like gradient coils are mounted on the outside of the magnet poles and utilize a closed-loop water cooling system for heat removal. The total gap between these coils, which is the space that is available for the patient, is 58 cm. Two shimming plates, an RF receiver channel and an integrated RF transmit coil and a portable RF shield are included. The magnet along with the gradient coils, covers, shim plates and the RF transmit coil weigh 430 kg and the total mass of the whole setup is 750 kg. The equipment area should at least measure to $5m^2$. There are several ready-to-use fast imaging sequences available with different spatial resolutions, contrasts and imaging times that can be selected from using the PC interface based on the neurosurgeon's needs [28].

An infra-red navigation camera mounted on a movable stand provides a registration between the position of the patient's head and the position of the magnet in 3D so that the neurosurgeon can see the actual position they are operating at and use the images displayed on the monitor to navigate their surgical approach to the tumour. The camera can sense the position of the magnet using five LEDs on each pole of the magnet [28].

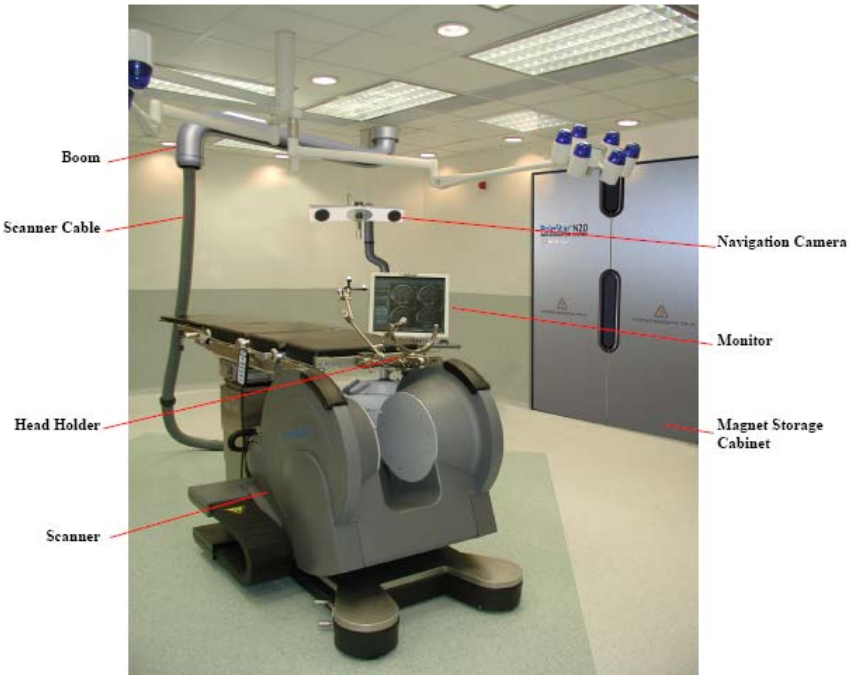

Figure 2.10: An overview of the components of the iMRI system. *Image taken from [28] - under Fair Dealing Exception permission [29]*

2.9 Promaxo: A Single-Sided Low-Field Prostate MRI Scanner

Promaxo is an office-based, FDA 510(k) cleared (2021), commercially available MRI scanner for producing images of the prostate and adjoining tissues [30,31]. This low-field MRI system is composed of an array of permanent magnets providing a constant in-plane magnetic field strength of 0.058 T - 0.074 T and a built-in z-gradient within its FOV. Promaxo uses gradient coils, RF transmission and receiver coils (the RF transmission coil has a peak power of 4 kW and the RF receive coil is patient wearable) along with other commonly used MRI components such as a spectrometer and signal amplifiers. In fact, Dr. Purchase helped MRI-Tech build a 4-kW RFPA for Promaxo [32]. There are multiple characteristics that differentiate Promaxo

from other MRI systems and the technology used on them including: Promaxo does not need a z-gradient coil as the z-gradient is built into the main magnetic field. The device utilizes a template holder for minimally invasive surgical procedures under MR guidance and it also includes an MR guidance user interface workflow. Promaxo also uses passive shimming [31, 33].

Figure 2.11: An overview of the Promaxo MRI system and its electronic rack including a graphical user interface (GUI). *Image and caption reproduced from article [34] with Creative Commons Attribution License permission from publisher: 'Cureus'.*

2.10 ULF Brain MRI Scanner

Yilong et al. (2021) [35] have recently reported the development of a low-cost, shielding-free ULF MRI scanner that does not require high power and uses permanent magnets. Their open double-pole magnet (saramium-cobalt is used to increase temperature stability) provides a homogeneous 0.055 T field and is used with linear imaging gradients. The whole magnet assembly weighs about 750 kg. They are also using a Electromagnetic Interference (EMI) cancellation technique, which is based on deep learning. Ten small resonant EMI-sensing RF

coils are used to eliminate the need for RF shielding by removing the external and internal EMI signals from MRI signals. These small coils are strategically placed near transmit and receive RF coils. To achieve a homogeneous field, additional passive shimming was also done. This ULF brain MRI scanner uses gradient field coils in x, y and z directions that are driven by a gradient amplifier. The G_x and G_y gradient coils were unshielded whereas G_z gradient coil was actively shielded. Anti-eddy plates were also utilized to reduce the eddy currents produced during the gradient pulsing. Separate transmit and receive coils were employed with the RF transmit coil having a solenoid structure and being driven by an extremely low RF power (11 W). The RF receive coil was a one-channel solenoid coil with an ellipse cross-section. There was also a decoupling circuit included to detune the receive coil during RF transmission. The RF signal input was amplified in two stages using a pre-amplifier with a +30 dB gain and in its second stage, the RF input was amplified +30 dB once again. A PC-based multi-channel NMR spectrometer console (EVO Spectrometer from MR SOLUTIONS [36]) with Powerscan v6.3 software was used for controlling the gradient and RF subsystems and data acquisition [35].

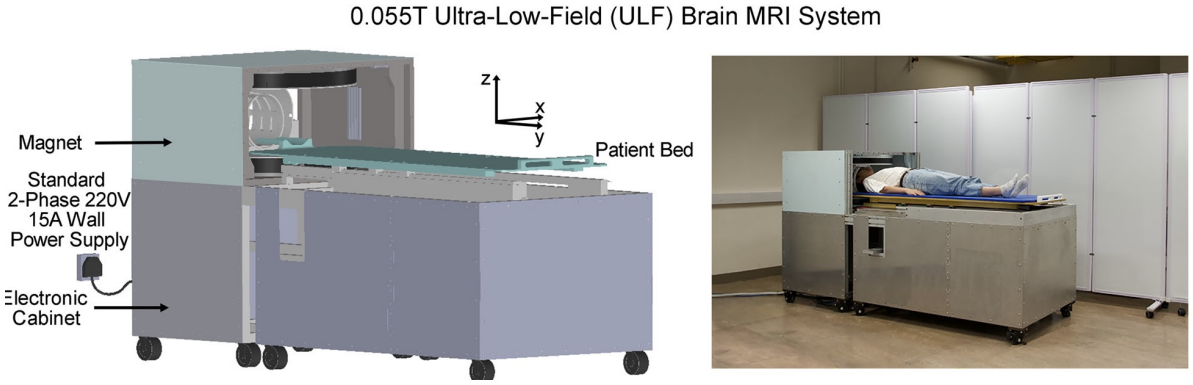

Figure 2.12: Prototype of an ultra-low-field (0.055 T) shielding free brain MRI scanner. *Image and caption reproduced from article [35] with Creative Commons CC BY permission from publisher 'Springer Nature'.*

2.11 Open-Access Imager (OAI)

Tsai et al. [6] developed an open access, VLF MRI system for in-vivo hyperpolarized ^{3}He (Helium-3) imaging of human lungs. This device is capable of imaging lung function in both horizontal and upright posture. A biplanar B_0 coil design with a magnetic field strength of 0.0065 T (6.5 mT) is used along with three sets of bi-planar gradient coils in x, y and z directions. The imaging subject is provided with a 79-cm inter-coil gap that allows imaging, which can benefit people who have asthma or obesity. Figure 2.13 shows an overview of OAI with its components. OAI uses an electromagnet design capable of generating a B_0 field as strong as 10 mT with a four-coil, bi-planar, 8th order magnet design in order to produce a homogeneous magnetic field over a large region. All four B_0 coils are connected to a single DC Power Supply Unit (PSU) which is constantly cooled by a recirculating power chiller [37].

To maintain the open-access, OAI team designed and constructed a set of planar magnetic field gradient coils in three axes with a minimum readout gradient field strength of 0.077 G/cm. The z gradients were based on a Maxwell pair configuration with additional correction loops. There were five loops in total for each plane with an inter-planar separation of 88 cm. The coils were wound around aluminum forms utilizing solid copper wire. The transverse gradient coils G_x and G_y were based on a planar projection from a cylindrical Golay coil. The optimal number of loops for each planar coil was five for each half. The eddy current potential has been minimized by assembling G_z frame using plastic and teflon spacers to prevent electrical contact between aluminum components. Each planar gradient set uses a Techron gradient amplifier [37].

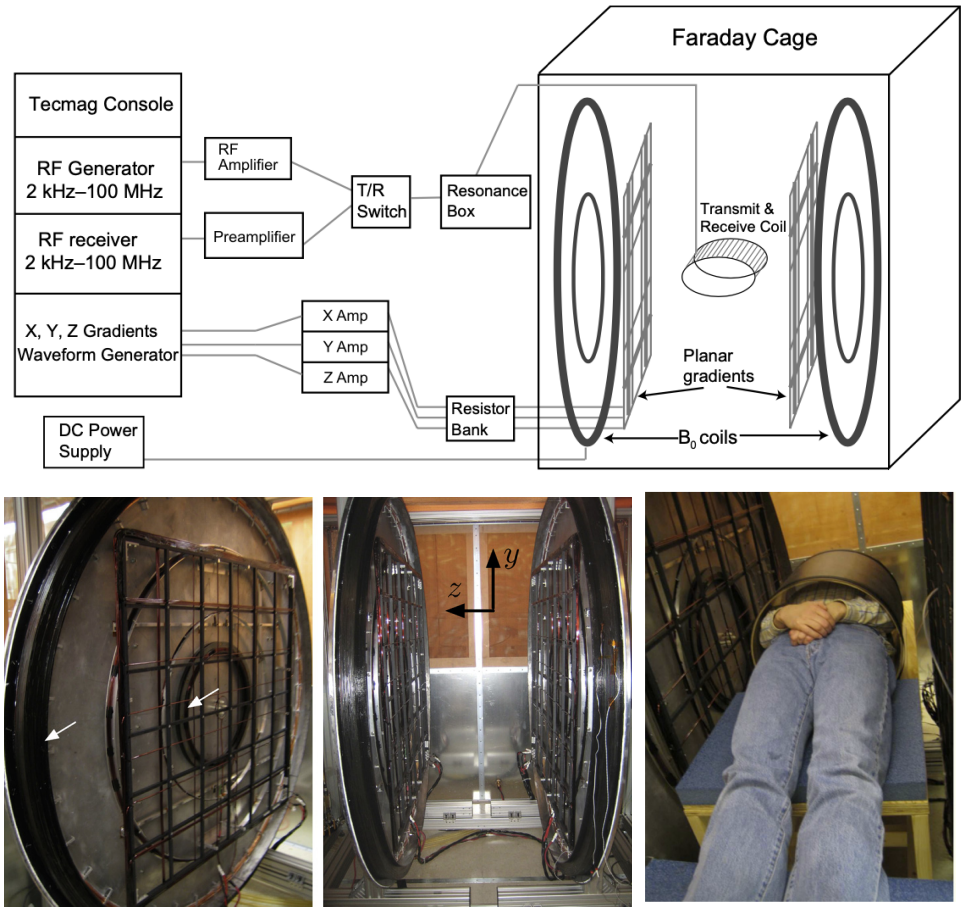

Figure 2.13: A schematic of Open-Access MR Imager (OAI) on the top and photos of OAI in the bottom. The right side photo at the bottom shows OAI with a patient in the supine position. Each coil and flange set has a combined mass of about 340 kg. *Image and caption reproduced from article [37] with permission (license number: 1252251-1) from publisher: 'Academic Press'.*

OAI also uses multiple solenoidal RF coils to fulfill different tasks including B_0 mapping, gradient field calibration, phantom NMR studies and human lung imaging. A chest coil large enough to the thoracic region was used for human lung imaging and a Bravo MRI impedance analyzer was used to test sample loading of the human chest coil. For RF and gradient pulse controlling and low-frequency signal reception, OAI uses an Apollo MR research console as its spectrometer. This system allows MRI at 210 kHz with no additional hardware needed. Besides, it includes an external gradient controller with three waveform generators that also

provide offset for x, y and shimming. An NMR plus amplifier is used for RF signal amplification across the range of 100 kHz to 1 MHz and includes blanking circuitry driven by the spectrometer. The amplifier is connected directly to a Transcoupler II probe interface that allows RF coils to function for both RF transmission and signal detection. OAI also uses a pre-amplifier with about +36 dB of gain to amplify the NMR signal before reaching the Apollo receiver. The OAI magnet, gradient and RF coils are placed inside a Faraday cage to prevent noise interference by up to 100 dB [37].

2.12 Portable MRIs with Non-Medical Applications

2.12.1 The NMR MOUSE

Eidmann et al. [38] designed an NMR imaging system in 1996, which they call a MObile Universal Explorer (MOUSE) due to its compactness and mobility. It has been developed for non-invasive investigation of arbitrary large objects. Although NMR MOUSE is not an MRI, it is one of the first one-sided magnets, therefore, it is historically important since there are one-sided magnets used in more recent devices such a The MR Cap and Promaxo. [32] In this device, RF generation and pulse programs are controlled by a PCB NMR console and the probe provides both B_1 RF field and the static B_0 field. A commercial low-field NMR spectrometer is used for the generation of the RF pulses, their amplification and signal detection. This spectrometer is controlled by a standard desktop PC. There is also a duplexer and a broadband 1 kW amplifier included in the setup. The pulse programs are written in Turbo Pascal and the NMR signals are acquired in quadrature which can be displayed and

stored by the PC [38].

The B_0/B_1 probe consists of two NdFeB alloy permanent magnets that can be positioned on the surfaces of random large objects and weighs about 2.5 kg. The RF coil is located in the gap between the two magnets that have a maximum field strength of 0.5 T. A four-layered solenoid with eight turns per layer is used for the RF coil. Eidmann et al. have demonstrated some potential applications of the NMR MOUSE by investigating various proton-containing samples and recording their SNR values in a table from an apple to a human hand [38].

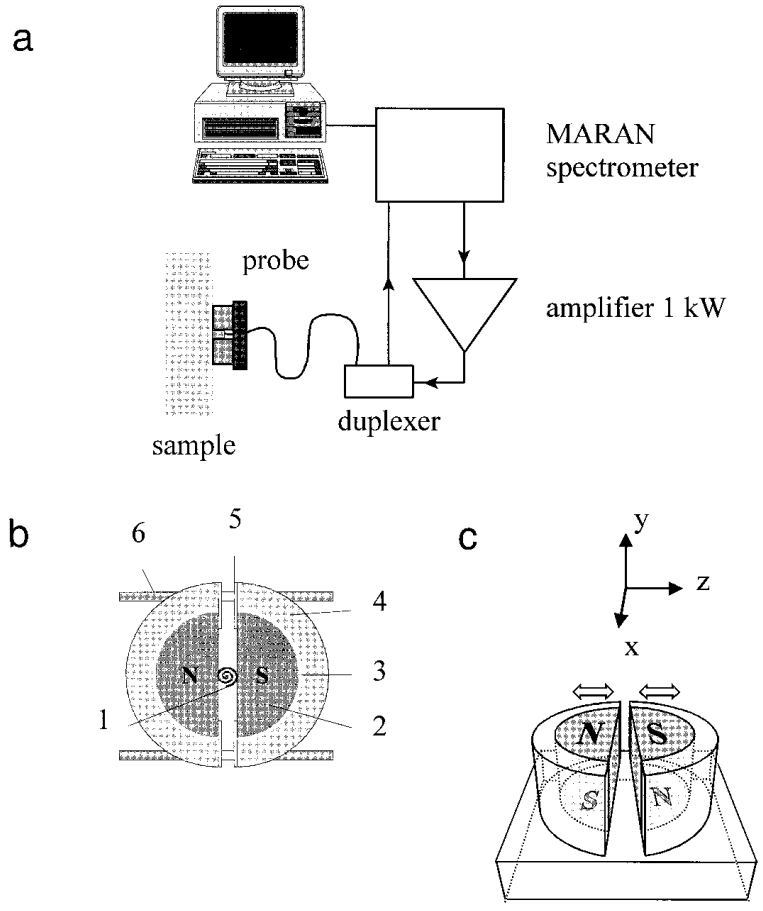

Figure 2.14: NMR MOUSE's setup. a, Spectrometer. b and c, Probe designs.*Image and caption reproduced from article [38] with permission (license number: 5357500126316) from publisher: 'Elsevier'.*

2.12.2 Portable MRIs for Trees

There have been multiple studies where plants have been studied outside of laboratories using portable MRIs including research done by Jones et al. (2012) [39], Kimura et al. (2011) [40], Hooman et al. (2007) [41], Rokitta et al. (2000) [42], Kockenberger (1997) [43], Van As (1984) [44], etc. Here, the MRIs exploited by the first two research groups are briefly discussed.

2.12.2.1 The Tree Hugger

Jones et al. (2012) designed the Tree Hugger for analysis of living forest trees in their original locations (*in situ* measurements). They utilized a transportable magnet that is uniquely designed to fit around a living tree and uses NdFeB magnets in its construction and weighs 55 kg (22kg magnetic material, 33 kg frame) [39]. The magnet looks like a traditional "C-core" in external appearance and has a central field strength of 0.025 T, but it does not feature a magnetic material return flux path. It can offer 210 mm diameter of open access space. The Tree Hugger uses conventional gradient coils with water-cooling pipes. The two gradient plates weigh 30 kg together and are capable of producing a field gradient of 1.06 mT/m/A for the z-gradient and 0.64 mT/m/A and 0.68 mT/m/A for G_x and G_y respectively. The MRI coil is a 14-cm standard solenoid winding which can be opened along its length to be wrapped around the tree. The RF electronics comprises a Maran DRX spectrometer and a 1 kW Tomco RFPA that weigh 46 kg together. There are also three in-house designed and built gradient amplifiers that generate 25 A pulses per channel at 30% duty cycle [39].

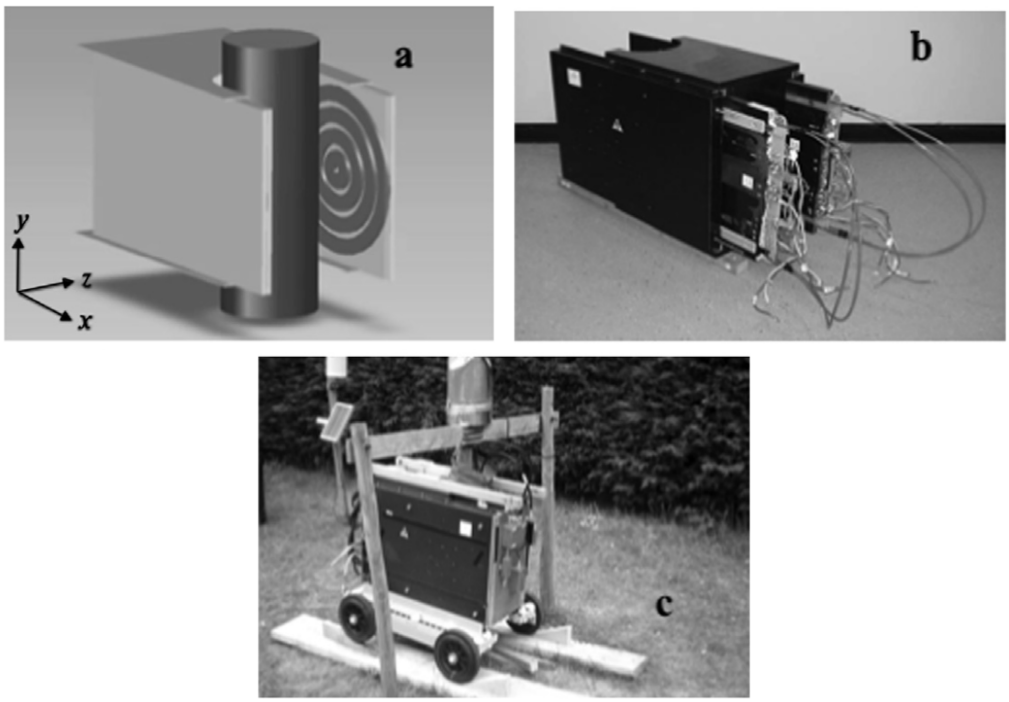

Figure 2.15: a, Represents a schematic of the magnet design showing open access frame of magnet with a mock tree between the poles. b, Shows the magnet as built with the gradient plates pulled half way out. c, Shows the magnet around a tree at Forest Research, Farnham, UK. *Image and caption reproduced from article [39] with permission (license number: 5417360889784) from publisher: 'Elsevier'.*

2.12.2.2 Mobile MRI system for Outdoor Tree Measurements

Kimura et al. (2011) developed an electrically portable mid-field MRI scanner with 0.3 T of field strength to diagnose diseased pear tree branches in a research orchard [16, 40]. The magnet was permanent and had a flexible rotation and translation mechanism. Their setup also included a probe with a local electromagnetic shielding, various electrical units, a mobile lift and an electric wagon. The device was capable of providing 2D cross-sectional images of the branches of a pear tree for measurements of T_1, T_2, proton density and apparent diffusion constant (ADC). The ADC map was used to successfully differentiate diseased from normal branches [40].

Their permanent magnet weighs 57 kg and was mounted on a turntable with two rotation axes and two horizontal sliding tables as it can be seen in figure 2.16. The centre of the magnet can be placed on any height of the object as long as it is below 160 cm from the ground. They had their 20 mm RF coil wounded directly around a pear tree branch and used a shielding cloth to shield both the RF box and the tree branch together. Also, they had their signal detection device installed in the gap of the permanent magnet (gap width: 80 mm). Their gradient coil set consisted of a planer transverse (G_x and G_y) and axial (G_z) traditionally designed coils. And they used an industrial PC with a Pentium 4 processor, an MRI transceiver, a transmitter and a three-channel gradient driver all together as their MRI console. The total weight of the MRI console together with the carrier it was installed on was about 100 kg [40].

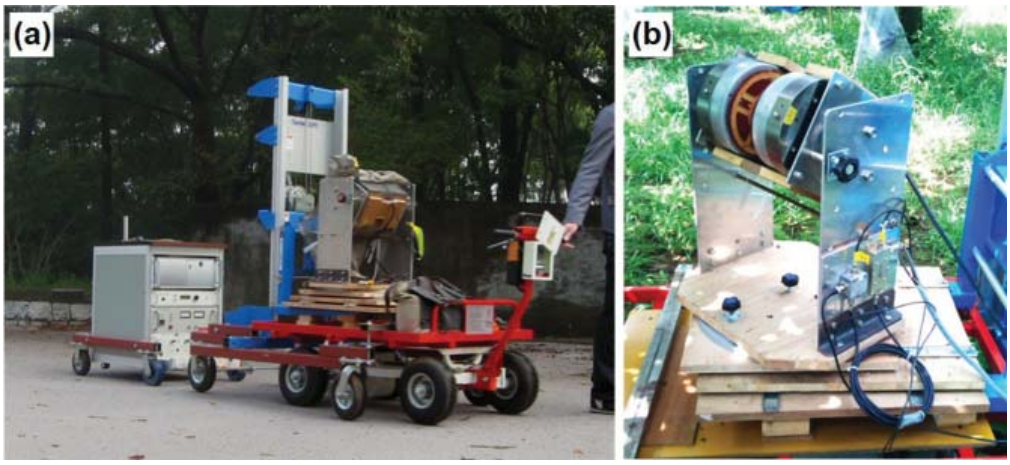

Figure 2.16: a, Overview of the plant MRI system developed by Kimura et al. b, The permanent magnet with its two rotational (both vertical and horizontal) axes and two horizontally sliding tables. *Image and caption reproduced from article [40] with permission (license number: 5357500619395) from publisher: 'AIP Publishing'.*

This chapter includes a range of different pMRIs built for different purposes and with different characteristics. There are mid-field pMRIs such as the Compact Hand and Wrist MRI built by Tereda et al., low-field pMRIs such as the MR Cap and ultra-low-field pMRIs

such as the 3D Brain and Extremity ULF MRI. The applications of these systems vary. Some of these pMRIs are used for diagnostic purposes in humans such as imaging the brain, human lungs and elbow injuries. There is also Medtronic iMRI that is used for navigation during neurosurgery. In addition, there are even MRI scanners that are created for facilitating assessments on living forest trees. The NMR MOUSE is also discussed briefly in this chapter. Although it is not an MRI scanner, The NMR MOUSE, an NMR imaging system which used a one-sided magnet for the first time and was built in 1996, is historically important. Most of the mentioned devices are developed more recently; such as Hyperfine's Swoop and Promaxo pMRIs that were built in 2020 and 2021, respectively. Although most of the discussed pMRIs are designed for low-field imaging, they are not necessarily light-weighted and most of them weigh over 100 kg. The lightest one of them is The MR Cap which weighs less than 10 kg while the heaviest ones are the Medtronic Polestar iMRI and the ULF Brain MRI scanner both weighing around 750 kg.

3 TRASE and Gradient-Free MRI

Magnetic Resonance Imaging (MRI) is a non-invasive, non-destructive diagnostic technique that delivers high-resolution in vivo images without relying on harmful ionizing radiations [45]. While Nuclear Magnetic Resonance (NMR) has been used since the late 1940's, MRI, which is in fact Nuclear Magnetic Resonance Imaging (NMRI), has only been around since the early 1980's. What differentiates an NMR instrument from a traditional MRI is gradient field coils. Without them, traditional MRIs are just NMR spectrometers [2].

In this chapter, a background of the theory behind how MRIs work is given. Since the principle of MRI is NMR, firstly, the theory behind NMR is briefly discussed, then traditional MRI scanners and their hardware is described. After that, gradient-free imaging methods are briefly mentioned, and lastly, a prototype of our portable MRI scanner is discussed and some comparisons between a conventional MRI scanner and our portable MRIs are given.

3.1 Background

3.1.1 Basis of Magnetic Resonance Imaging (MRI)

Nuclear Magnetic Resonance (NMR) is a phenomenon that occurs due to atomic nuclei spinning about their axes and generating their own magnetic moment [46]. In order for NMR to happen, there should be a resonance transition between magnetic energy levels in

a nuclei when it is in the presence of an external magnetic field and is exposed to an RF radiation. [47].

Some of the important nuclei for organic compounds such as hydrogen, carbon and nitrogen have nuclear spins since they have an odd number of protons and/or neutrons and therefore they respond to this technique. This is important because it makes it possible to observe the internal structure and function of human body by using the NMR technique [46]. However, the spin of these nuclei would stay randomly oriented unless there is an external magnetic field present. This applied external magnetic field is referred to as B_0 in NMR. From quantum theory, the number of energy states of a nucleus corresponds to its spin quantum number S by= $2S+1$ [48].

For instance, for a hydrogen nucleus which is a single, positively charged proton with a spin S=1/2, in the presence of a strong B_0, two orientations are possible for the nuclear spins. They will align with the external magnetic field by either becoming parallel to it in the same direction or by orienting against it. These two possible spin states are shown as +1/2 spin state and -1/2 spin state. In +1/2 state the spin has the same direction as B_0 and has slightly lower energy. And in -1/2 spin state it has the opposite characteristics of the former one [49]. The energy gap between these two states, ΔE, depends on the strength of the external magnetic field, the stronger B_0 is, the greater the ΔE becomes.

When an ensemble of protons are placed in the presence of a strong external magnetic field B_0, they line up with B_0 and generate a net magnetization M_0. As well as spinning about their own axis, when these protons are placed in the presence of an external B_0, they start to precess about the axis of B_0. Electromagnetic radiation in the RF region can provide the required energy to excite the proton from the +1/2 state to the -1/2 state. If this energy

matches ΔE, the proton then is able to go into resonance with the electromagnetic radiation by absorbing this energy and flipping its magnetic moment from the lower energy state to the higher energy state [46]. In other words, if the Larmor frequency (ω_L) of a proton, which is the number of times per second that the proton precesses in a cycle, matches the frequency of the electromagnetic (EM) radiation, resonance occurs. Therefore, the frequency of this electromagnetic radiation depends on both the strength of B_0 and the type of nuclei present [49]. The Larmor equation is:

$$\omega_0 = \gamma B_0 \tag{3.1}$$

in which ω_0 stands for angular precessional frequency of proton and γ is the gyromagnetic ratio.

This phenomena is important because once the nuclei are placed in a strong magnetic field and are exposed to pulses from an RF radiation with their Larmor frequency, they get excited. This makes them flip their magnetic moment. When the RF field gets turned off, the energy is released as the protons realign with B_0 [49, 50]. The way in which the spins of nuclei interact with their environment or neighbouring magnetization can be described by two relaxation terms T_1 and T_2. These terms describe the time it takes for a nucleus to return to its equilibrium state after being excited by an RF signal and the different properties of various tissue types cause T_1 and T_2 to vary. Consequently, T_1 and T_2 can be used to distinguish between different tissue types and create contrast in images.

3.1.2 Spatial Encoding and Imaging

The signal that is coming from the nuclei in the sample can be detected by an RF receiver coil. This detected signal is called a free induction decay (FID) and will be the integral of the magnetization over the FOV. It would is the strongest for a 90° flip angle pulse and can be used for spatial localization and reconstructing an image. This requires a method for determining the spatial origin of the signal.

A spatially varying field in the x, y and z directions needs to be present in the sample so that the nuclei can generate signals with information about their locations. This information can be encoded with or without the usage of B_0 gradient coils. B_0 gradient coils generate gradient fields with spatially varying magnetic field strength over the sample. 3D spatial encoding with B_0 gradients is usually done using slice selection (G_z), frequency encoding (G_x) and phase encoding (G_y) methods. The mathematical representation of these three B_0 gradients is: $G_x = dB_z/dx, G_y = dB_z/dy, G_z = dB_z/dz$. When using a slice-selective gradient along the z direction, which is parallel to the B_0 field, a spatially varying Larmor frequency of the spins is created along the z direction. By adjusting the RF transmit frequency, a particular slice of the subject being imaged can be selected. The received signal will be an integration over spins in the selected slice. After selecting a slice, 2D spatial information can be encoded into an image using frequency and phase encoding gradients. Frequency encoding is done by applying a linear B_0 field gradient along the x direction. This causes the nuclei in the sample to have different precession frequencies depending on their location along the encoded direction. The precession frequency is directly proportional to the strength of the magnetic field, and therefore, the position of the nuclei in the selected direction. Similar to

frequency encoding, in phase encoding a linear B_0 field gradient along the y direction causes the spins along that direction to precess faster on one end than the other end. Once this gradient is turned off, the nuclei along the y direction return to precessing at their original precession frequency, but with a phase offset. This phase offset creates a phase gradient along the y direction.

Spatial encoding without B_0 gradient coils can also be done in various ways including B_1 magnitude gradient and B_1 phase gradient. Methods that utilize the magnitude gradient of the B_1 field include rotating frame imaging and *Bloch-Siegert (BS)* spatial encoding. TRASE and non-linear RF phase encoded MRI are methods that use B_1 phase gradients to encode the spatial information. TRASE will be discussed more in the coming sections [51–53].

Rotating frame zeugmatography was an early RF imaging technique, D. I. Hoult published his paper on this technique in 1978. This method keeps the sensitivity of the 2D Fourier transform while omitting the need for any gradient field changes. In this method, a homogeneous field plus a gradient in the amplitude of the RF field was used for spatial encoding. This method depends on large flip angle pulses and requires high RF power and takes a very long time since every single data point is collected one at a time after each excitation pulse is sent [51, 52].

Bloch-Siegert spatial encoding introduces a spatially dependant phase shift to the on-resonant transverse magnetization by applying far off-resonant RF pulses. This phase shift is called BS and it is the basis of this type of encoding. Although BS creates a phase shift in the transverse magnetization, it does not significantly tip the magnetization vector. Adapted RF coils with a linear shaped B_1-field and a homogeneous B_0 field make it possible to use this shift towards spatial phase encoding. The BS Spatial Encoding Technique (BS-SET), has

been used to produce 2D images on a 0.5 T system utilizing an adapted image reconstruction technique [53].

Rabi encoding is another gradient-free MRI method that uses frequency modulated echoes. Frequency-modulated Rabi-Encoded Echoes or FREE uses Adiabatic Full Passage (AFP) pulses and a B_1 gradient field to generate spatially dependant phase modulation. FREE encodes spatial information in the phase of the magnetization with its signal intensities minimally affected by resonance offset. This is important because other methods such as rotating frame zeugmatography are limited by their sensitivity to resonance offset. FREE also claims to make multidimensional MRI feasible when combined with conventional frequency encoding using a B_0 gradient [54]. Comparing these gradient-free methods, TRASE is the least complex method hardware-wise with fairly high resolution compared to the other ones [32].

3.2 Conventional MRI Setup

In summary, image production in MRI happens by recording spatially encoded phase and frequency data in the NMR signal. Then the signal is converted into an image using the computer's signal processing algorithms [55]. In traditional clinical MRIs, flowing current in the main field coils produces the main magnetic field which is denoted by B_0 [2]. In spite of all the advancements that have been made in the quality of the images that are acquired using this method, the basic technology has remained the same throughout the decades [56].

Generally, commercial MRI scanners consist of five main components:

- A magnet to generate the main magnetic field B_0 of 1.5 or 3.0 Tesla (T) [57]
- Gradient field coils which produce linear B_0 gradients to facilitate the spatial encoding

and gradient coil amplifiers.

- RF transmit and receive coils to produce the B_1 magnetic field and manipulate the spin and receive the MRI signal, Low Noise Amplifiers (LNAs) and RF power amplifiers which are the focus of this thesis and will be discussed in detail later.

- The MRI control console which is used to acquire and store the data [2].

- Shim coils to make the main magnetic field as uniform as possible for MRIs that use uniform B_0 fields [2].

More than 75% of the magnets used in the construction of conventional MRI scanners that are installed annually are either 1.5 T or 3.0 T superconducting magnets (over 70% of which are 1.5 T scanners) [58]. Superconducting magnets do not have resistance to electricity like regular magnets, which means that using them saves a lot of power and prevents heat generation. In the past, superconducting magnets used to be made of a series of coils with a cylindrical form inside a bath of liquid helium enclosed in a cryostat. However, more recent superconducting coils use the new high-temperature superconductors [32]. Superconducting coils can maintain the magnetic field strength when the current is flowing through them, as long as the magnet is being cooled properly. Increasing the magnetic field strength will increase the longitudinal magnetization. This happens as a result of more protons aligning along B_0. This leads to more SNR, which improves spatial resolution and speed in imaging [55]. Table 3.1 shows some typical parameters of cylindrical superconducting MRI magnets [59].

To spatially encode the MR signal and localize it to a specific region in space, conventional MRI systems use gradient coils. Although there are imaging methods that do not require the

Magnetic Field Strength	**1.5 T**	**3 T**	**7 T**	**11 T**
Length, cm	125-170	160-180	∼300	400
Outer Diameter, cm	190-210	190-210	>250	460
Stored Energy, MJ	2-4	10-15	50-90	340
Weight, ton	3-6	5-10	>25	150

Table 3.1: Typical parameters of cylindrical MRI magnets. [59] *Copyright ©2011, IEEE*

usage of gradient coils, these components are important parts for traditional MRIs [55, 60]. Gradients create an additional magnetic field on top of B_0 that has a varying strength along the gradient's direction. To be able to produce an image of an object/a patient using the MR signal, a set of coils need to be installed around the subject. These make it possible to choose a specific slice within the object/body. Gradient coils produce three linear B_0 gradients (G_x, G_y, G_z) which affect the resonant frequency based on spatial position and time [55, 61].

MRI scanners use RF coils to send RF pulses and receive the signal back during imaging. RF coils play an important role in determining SNR and signal uniformity. In conventional MRIs RF pulses flip the magnetization away from the z-axis by tilting the magnetization by either 90° or 180°. There are transmitter RF coils, receiver RF coils or transmitter/receiver RF coils. RF coils produce a magnetic field called B_1 which is perpendicular to the B_0 field. Volume coils and surface coils, which are two basic types of RF coils, each have different applications [55].

The aforementioned pulses that are generated by gradient and RF coils require computer systems for controlling. An MRI console has more functions including data collection and image generation and display that can happen using an automated post-processing analysis software [55].

3.3 TRansmit Array Spatial Encoding (TRASE) MRI

Although gradients are the parts that set traditional MRIs apart from NMR spectrometers and enable us to acquire images, they are also the parts responsible for the loud acoustic noise of an MRI scanner. The fast switching of gradient coils is responsible for the generated noise [2]. These pieces of hardware consume a lot of power, require air and water cooling systems for their complex electronics and occupy a great amount of space. Consequently, a large amount of the costs incurred by MR systems is due to having MR field gradients on site. Not only are these expensive components, but also the price of installation of the system and post-installation maintenance are high. Additionally, the complexity of operating an MR system creates more complications. Besides, gradients can induce unwanted eddy currents in patient's body and other nearby conductors. Hence, eliminating these parts can make significant improvements regarding the cost, weight, and complications of an MRI system [61].

Nevertheless, it is worth mentioning that cooling is not a major issue for the low-field MRI systems such as the ones reviewed in the previous chapter and the amount of power used can be reduced. However, all of those MRI systems still have gradient coils, therefore, eddy currents and complexity of the system are issues that apply to low-field MRIs as well as large, high-field ones.

Dr. Jonathan C. Sharp, one of my advisory committee members, is a co-inventor of a novel technique which does not require the usage of field gradients. TRASE is a silent imaging technique based on phase gradients of the RF field that functions entirely without a B_0 gradient field [61]. TRASE utilizes echo-train pulse sequences and uses linear RF phase

gradients instead of magnetic field gradients to produce Fourier spatial encoding equivalent to conventional MRIs [61,62]. The magnetic component of the RF field is called B_1 and TRASE-based gradient-free MRIs use B_1-encoding instead of B_0-encoding (used in traditional MRIs) [2]. To encode a spatial axis, two different RF phase gradient fields are applied in alternation as 180° refocusing pulses. This results in progressively increasing high-resolution data moving down the echo train. Hence, a long echo train correlates with high spatial resolution and image resolution is limited by how long the echo train is. In certain regimes very high-resolution imaging is also possible. The stronger the phase gradient is, the higher the image resolution will be. This is determined by transmit coil geometry [62].

Using TRASE makes it possible to have high-resolution, portable MRI systems at a cheaper price. This facilitates access to these machines for more people, especially people who live in more deserted areas. It can provide useful diagnostic information when used in emergency rooms as a portable system, without having any ionizing radiations. Using TRASE has also brought us closer to having means of monitoring the health of muscles and bones of astronauts during their space missions. This is because "Owl" and "Merlin", the gradient-free TRASE-based portable MRIs that teams at the Space MRI Lab at the University of Saskatchewan (Usask) have been developing for the past few years are meant for space applications.

3.3.1 TRASE In Different Dimensions

The MRI signal is acquired in k-space during the frequency encoding after applying the slice-selective and phase encoding gradients. K-space is a multidimensional data matrix and is defined as the integral of B_0 gradient over time. In k-space, k_x represents frequency encoding,

k_y represents phase encoding and k_z represents slice-selective gradients. Each point in k-space represents a specific combination of frequency and phase information for a given location in the image and Fourier transform is what connects the k-space and the image domains. The k-space data is normally acquired in a specific sequential manner, with the data being acquired at different locations in k-space by changing the gradients. An inverse Fourier Transform (FT) can then be applied on the collected 2D k-space data to determine the signal from a point (x,y) in a 2D plane and be represented as a pixel in the MRI image.

1D TRASE k-space encoding requires two coils. In this method, a 90° excitation pulse is followed by a sequence of 180°refocusing pulses alternatively applied to A and B coils. After each of these refocusing pulses, an echo is collected. Figure 3.1 shows how the k-space is collected in one dimension using TRASE technique.

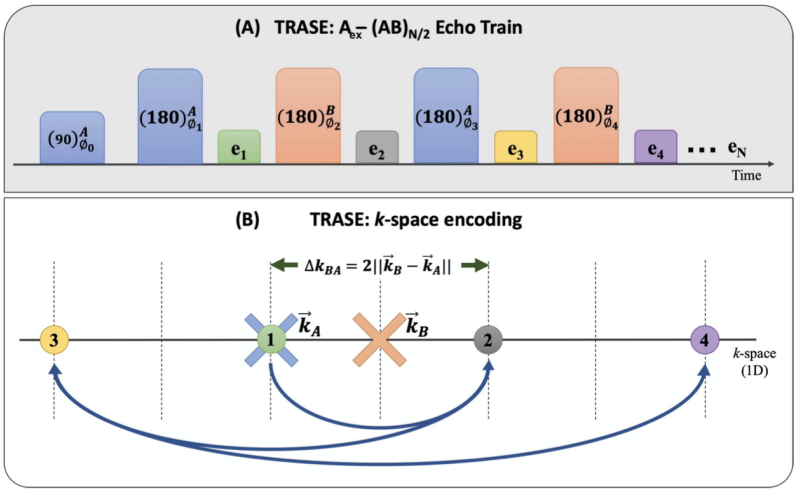

Figure 3.1: One dimensional k-space encoding in TRASE. A, Shows an echo train used for TRASE in 1D in which an initial 90° excitation RF pulse is followed by 180° refocusing pulses. The refocusing pulses are applied to the first and the second coils called A and B alternatively and an echo is collected after each refocusing pulse is applied. B, The sampling pattern used to collect the k-space data in 1D with TRASE is shown. In this picture, the crosses represent the k-space coil origins and the numbered circles show the travelling pattern of the echo train in k-space [63]. *with permission (license number: 5475720494151) from publisher: 'Elsevier'*

TRASE encoding can also be done in two dimensions, however, this requires at least three B_1 phase gradients in different non-parallel directions on a 2D plane. Figure 3.2 shows how adding a third TRASE coil, C, with k-space origin k_C makes 2D encoding possible. This setup requires an initial 90° RF pulse followed by 180° refocusing pulses. Figure 3.2 shows some examples of possible k-space trajectories for 2D TRASE imaging. ITheoretically, in order to encode spatial data in a 3D volume with TRASE, a fourth TRASE coil with a k-space origin that is not on the same plane as A, B and C coils is required (all four coils need to be noncoplanar and noncollinear). However, there are many obstacles in the way of building pure 3D TRASE MRI systems, such as the data acquisition time being too long for *in vivo* imaging and the fact that high resolution 3D TRASE can require up to six different B_1 fields. Nevertheless, slice-selective 2D TRASE is a reasonable compromise for 3D TRASE that can still prove valuable for clinical use. In this method, RF phase gradients are used for slice selection to define imaging planes. In TRASE slice selection, small flip-angle excitation pulses are applied between refocusing pulses. [64]

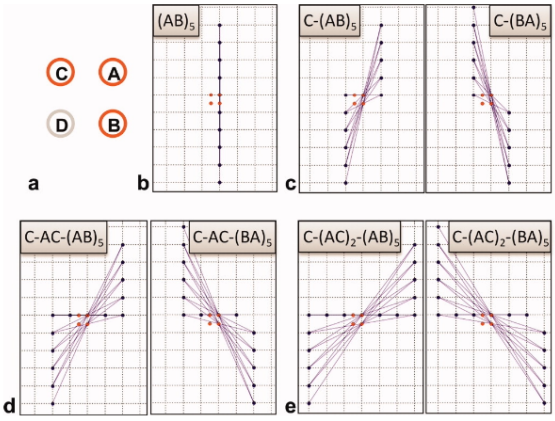

Figure 3.2: Some examples of k-space trajectories for two dimensional encoding in TRASE. a, B, C and D represent the k-space origin of four fields where the coil A has been used for excitation in all cases and the coil D has not actually been used. b, To scan a vertical k-space line, sequence $(AB)_5$ is used. c, The first pair of vertical lines are scanned with $C-(AB)_5$ and $C-(BA)_5$ sequences. d, The second pair of lines can be acquired using $C-AC-(AB)_5$ and $C-AC-(BA)_5$ sequences. e, $C-(AC)_2-(AB)_5$ and $C-(AC)_2-(BA)_5$ give a third pair [64]. *with permission (license number: 5475750287166) from publisher: 'John Wiley and Sons'*

3.3.2 TRASE MRI Versus Conventional MRI

As mentioned earlier, TRASE uses phase gradients of the RF field for spatial encoding [62]. It eliminates the B_0 gradient coils and all the issues associated with them, nevertheless, it creates new obstacles that need to be overcome. This gradient-free method requires multiple, short, high-power RF pulses that facilitate the collection of as many k-space data points as possible within the T_2 decay window. It utilizes multiple RF coils with different phase gradients to traverse further in k-space by using refocusing pulses. In one-dimensional (1D) TRASE, a single 90° excitation RF pulse is followed by multiple high-power 180° RF refocusing pulses. The acquired signal between each refocusing pulse gives a single data point in k-space. More RF coils are needed for TRASE in two and three dimensional imaging [65]. Figure 3.3 shows a comparison between the k-space behaviour of a conventional B_1 coil used in traditional

MRI systems and a phase gradient B_1 coil that is used in TRASE [66]. Figure 3.4 represents the components of a conventional MRI scanner and a 1D TRASE MRI scanner and their relationships.

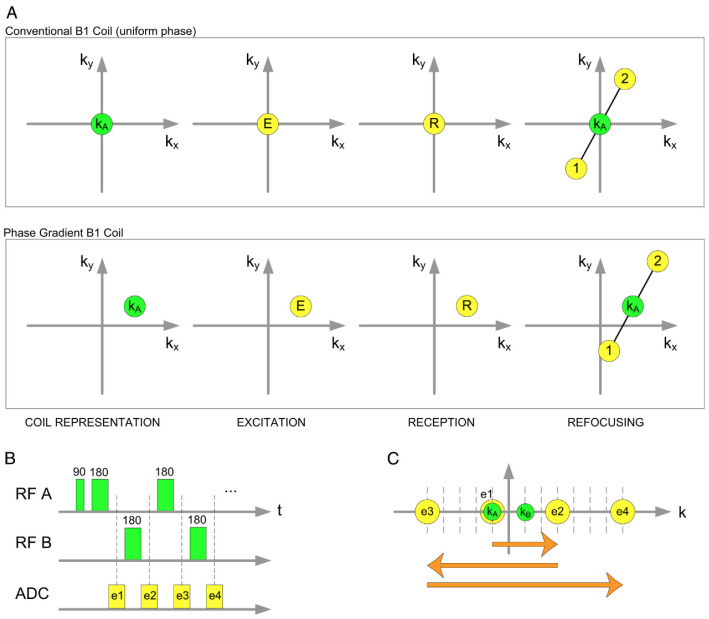

Figure 3.3: A, Shows how a conventional B_1 coil behaves in k-space in comparison to a phase gradient B_1 coil. In this image, K_A represents the k-space origin of the coil. In traditional MRI scanners, the centre of k-space is the same as k_A. Because in conventional coils, the phase gradient has zero strength. Contrarily, when there is an RF phase gradient field present, the coil k-space origin will not be the same as the k-space origin and k_A can be shown as a point in k-space. E in the second panel represents excitations of the spins to the coil k-space origin. The phase gradient of the receive coil is what determines the location of a an acquired signal in k-space. The fourth panel represents the transformation of an initial k-space state shown as '1' to a different state marked as '2'. While this translates to a point reflection in the k-space origin for conventional MRIs, this is not the case in TRASE RF encoding. This is due to the k-space origin not being the same as the transmit coil k-space origin because of the phase gradient coil's presence. B, To encode spatial information in one dimension, TRASE needs two transmit fields (RF A and RF B) with distinct k-space origins. The first 90° pulse is the excitation pulse and it is followed by multiple 180° refocusing pulses. e_1, e_2, etc. represent the echo data that are being acquired after each refocusing pulse. C, Represents the k-space location for each echo. *Image and caption reproduced from article [66] with permission (license number: 5357510225474) from publisher: 'Elsevier'.*

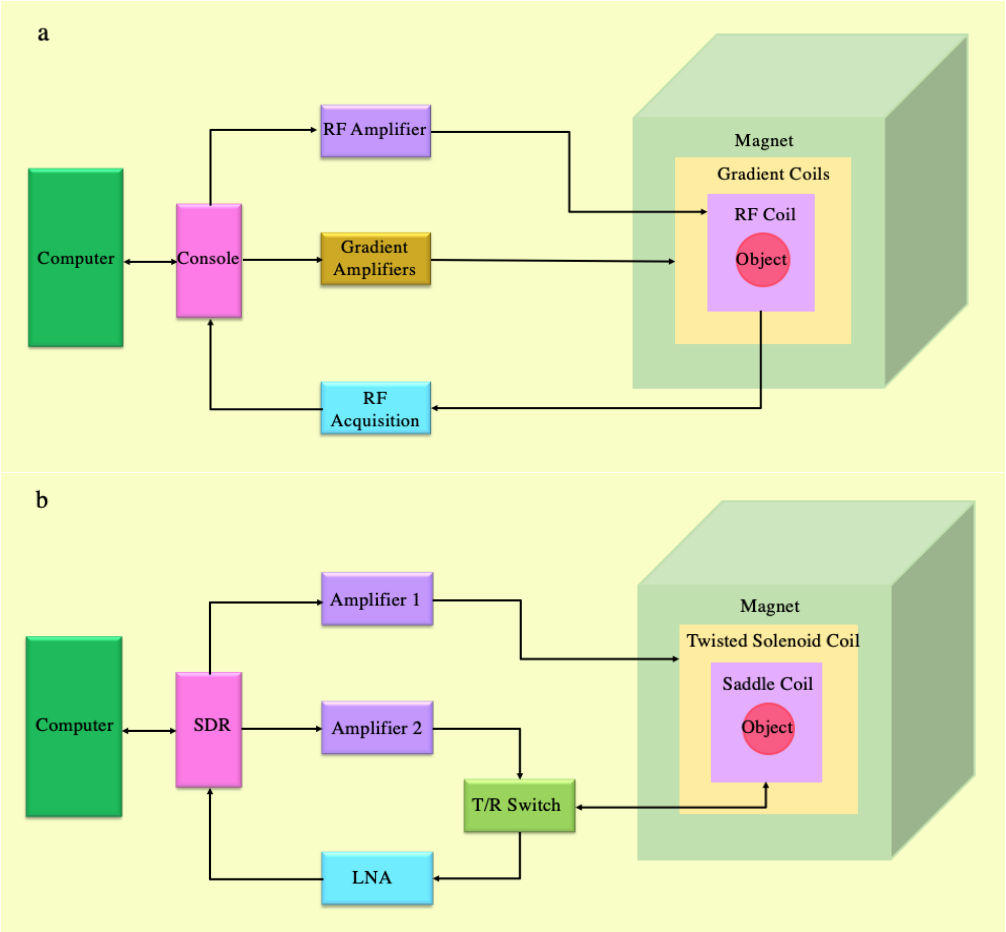

Figure 3.4: A comparison between conventional and TRASE MRI scanners. a, Shows a block diagram of different components of a conventional MRI scanner, their relations to each other and how magnet, gradients and RF coils are normally set in a conventional MRI system. b, shows a block diagram of a 1D TRASE-based, gradient-free MRI scanner.

3.3.3 The Merlin MRI Setup

The Merlin is an ankle-sized gradient-free MRI that uses both B_0- and B_1- encoding and has a built-in gradient in the B_0 field in one direction leading to natural slices. This makes Merlin's B_0 field non-uniform by design, therefore, shimming is not required in the Merlin. This TRASE-based MRI scanner was constructed to image upper ankle area with fundings from the Canadian Space Agency (CSA) to be used on astronauts in International Space

Station (ISS) and was flown on a Falcon 20 jet for zero-gravity testing; it takes its name, Merlin, from the fact that Merlin is a kind of falcon bird. It works with 2D TRASE encoding and natural slice selection using magnet blocks with a Halbach magnet arrangement that have an in-built gradient in the SMACS y direction. SMACS stands for the Standard Merlin Awesome Coordinate System which is defined with the origin being set at the centre of the magnet; x-axis is defined form left to right, z-axis is defined from bottom to top and y-axis is defined from front to back. Figure 3.5 shows the SMACS. B_0 is in z direction and is approximately ∼633 Gauss (63 mT, 2.69 MHz). Merlin uses 312 NdFeB grade N52 block magnets of 2.54 cm x 2.54 cm x 1.72 cm dimension that weigh 62 g each, leading to a total weight of 23 kg. The Merlin MRI scanner uses three TRASE coils including a saddle coil, an x-twisted solenoid coil and a z-twisted solenoid coil. Here, x-twisted solenoid coil means it has a phase gradient in the x direction and a z-twisted solenoid coil means having a phase gradient in the z direction.

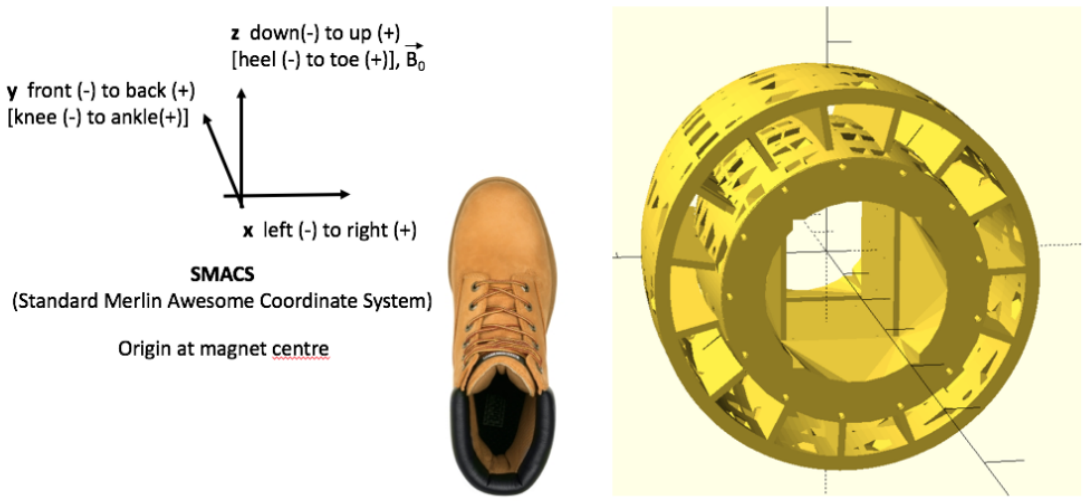

Figure 3.5: The Standard Merlin Awesome Coordinate System (SMACS). *Permission from Dr. Sarty [32]*

Tuning and matching circuits were mounted on the Merlin MRI RF coils. Initially class

D amplifiers were being used on Merlin, which then later changed to class A/B AN799H amplifiers due to the class D amplifiers' technology leap which will be discussed later in this thesis. The Merlin uses SDR_8R_8T for its SDR designed to have eight transmit and eight receive ports. RF Transmit (Tx) and RF Receive (Rx) coils require a Tx/Rx switch, and the switch used on the Merlin MRI scanner followed the same design as the Owl MRI, another one of the Space MRI Lab's TRASE MRI scanners. Also, the Merlin uses a ThinkPad laptop to control the SDR. In April 2021 Merlin was successfully tested in zero-gravity on the aforementioned Falcon 20 jet in one of National Research Council (NRS) centres in Ottawa and demonstrated $\sim$ 80% readiness and robustness for the hardware used in our TRASE-based prototype space MRI scanners [67]. Table 3.2 compares different components of a conventional MRI scanner to the components our TRASE-based gradient-free MRIs use in their design.

	A Conventional MRI Scanner	A TRASE MRI Scanner
Magnet	Most of them use superconducting permanent magnets to create homogeneous fields and require 1.5 or 3.0 T magnetic field strength and weigh between 3 to 10 tons [59].	Use light-weight and low-field (∼60 mT) permanent magnets and make inhomogeneous fields.
Gradient coils and Their Amplifiers	Use power-hungry, heavy and loud gradient fields with their amplifiers. Gradient coils produce three linear B_0 gradients (G_x, G_y, G_z). In standard clinical MRIs, the slice selection gradient coil is the magnetic field gradient along the z-axis, the phase encoding gradient is G_y and the frequency encoding gradient is G_x [55].	Use built-in gradient fields which makes them simple, light-weight, robust and portable and eliminates the noise and the need for gradient coil amplifiers.
RF Transmit and Receive Coils	Conventional MRI scanners use these coils for transmission and reception of the RF signal (To create the B_1 field and receive the MR signal).	Similar to conventional MRI scanners, our TRASE MRI scanners also use Tx/Rx coils but the transmit coil has to have a specific design to produce the B_1 phase gradients required for TRASE encoding. The number of coils depends on the number of dimensions the imaging is being done at.
Tx Amplifiers	The transmit signal needs to be amplified before being sent and to do so, conventional MRI scanners use commercially available amplifiers.	TRASE requires fast switching between its RF transmit coils, which means an amplifier with a high duty-cycle is needed that can also provide an appropriate amount of SNR, and since the commercially available amplifiers are not able to provide this, specific designs are used to fulfill this aim.
Rx Chain (LNA)	In both situations receive chain electronics are needed and frequency considerations might affect the choice of components such as the selection of the suitable LNA (Low-Noise-Amplifier). For instance, the Owl uses a commercially available MITEQ RF amplifier as an LNA for its receive chain.	
The Console	An MRI console has functions including data collection and image generation and display that can happen using an automated post-processing analysis software [55]	TRASE is also a Fourier-based imaging technique and does not require any specific image processing techniques that differ from what conventional MRI scanners use. However, the console needs to be capable of generating various control signals for components such as gating circuit and RF input pulse which is done using SDR and FPGA technology.

Table 3.2: A comparison between the typical components of a conventional MRI scanner and a TRASE MRI scanner such as the Owl and the Merlin [59]. *Copyright* ©2011, IEEE

As mentioned earlier, using a new technology like TRASE introduces new requirements.

One of these essential requirements is a different version of RF power amplifiers that are needed for any MRI system to work. This is required for high-resolution imaging and since there are no commercial RFPAs with a high enough duty cycle and high power output that can generate multiple, short, high-power RF pulses needed for k-space data point collection, there is a need for a new design for an RFPA that is compatible with TRASE [65].

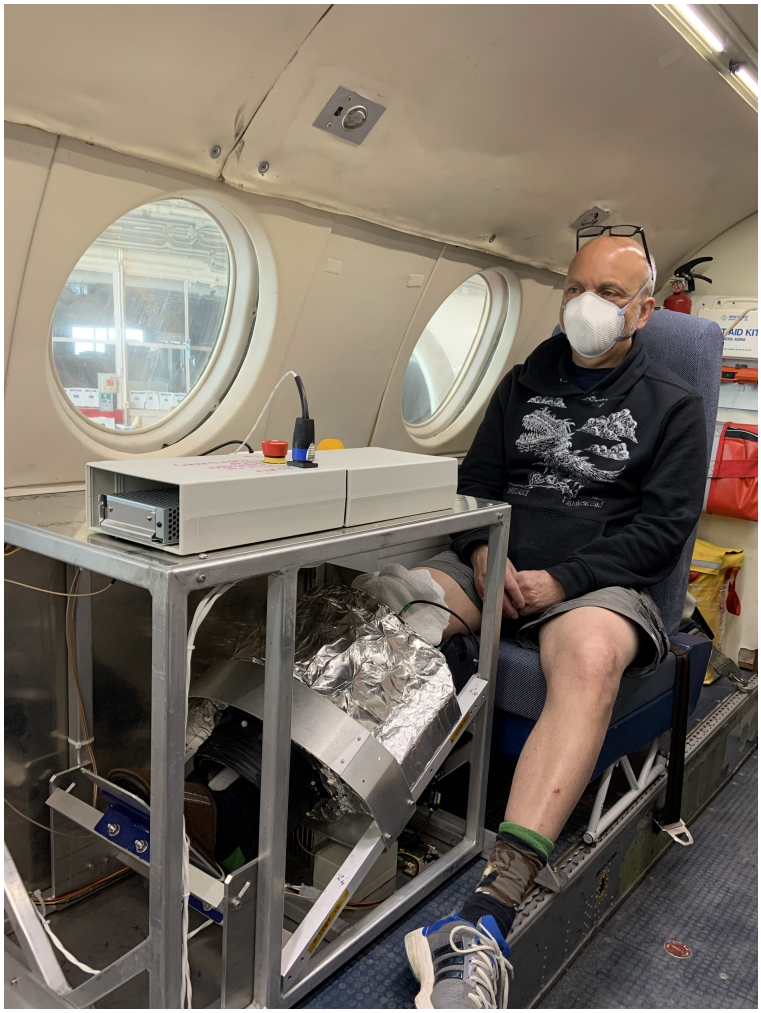

Figure 3.6: The Merlin MRI on a Falcon 20 jet being prepared to be tested in zero-gravity. Dr. Gordon Sarty's right ankle is inside the Merlin in this photo. The aluminum RF shields are not used here. *Photo taken by the author.*

4 Amplifiers for TRASE MRI

4.1 Background

An RFPA is defined as a device that can amplify an input RF signal into an RF output signal with reasonable linearity and efficiency. RFPAs can be put into two main categories based on their attempt to preserve the original waveform of the input RF signal at the output. The RFPAs that make such attempt are considered linear and the ones that make no attempt to preserve the initial waveshape are considered nonlinear amplifiers [68]. While a small signal amplifier or a voltage amplifier increases the voltage level of the input signal, a power amplifier boosts the power level of the input signal. Power amplifier design is also similar to LNA design in some respects [69]. The trade-offs involved in the design of RF circuits can be explained and summarized in figure 4.1 that shows the "RF design hexagon". Almost any two of the six parameters in the diagram trade with each other in some way [70].

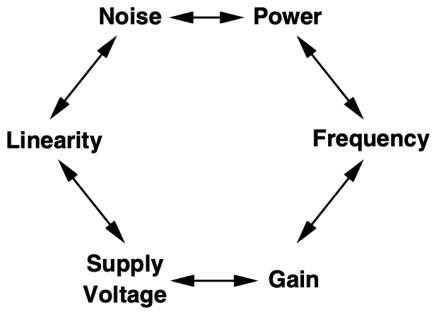

Figure 4.1: RF design hexagon. *Images taken from [70] Permission granted through email communications with the publisher*

4.1.1 RFPA Characteristics

RFPAs are also put into different sub-divisions or classes based on their circuit configurations, linearity and efficiency [68]. In designing RFPAs, the main trade-offs are amongst linearity, power gain, output power and efficiency. In this section, these performance metrics are defined.

4.1.1.1 Efficiency

Since power amplifiers are the most power-hungry blocks in RF transceivers, they need to have high efficiency. Another critical performance metric for a PA is its gain. While an amplifier's efficiency describes how well it can convert DC input power to RF output power, its gain depends on how well it can convert an input RF power to output RF power. The efficiency of a PA can be defined by its drain efficiency [70]:

$$\eta = \frac{P_{Out,RF}}{P_{In,DC}} \tag{4.1}$$

where $P_{Out,RF}$ or P_L is the average power delivered to the load and $P_{IN,DC}$ or P_{supp} is the average power drawn from the supply voltage.

Power-added efficiency (PAE) is another way of describing efficiency for cases where the power gain is relatively low; this quantity embodies this effect and is defined as [70, 71]:

$$PAE = \frac{P_{Out,RF} - P_{In,RF}}{P_{In,DC}}, \tag{4.2}$$

where $P_{In,RF}$ is the average input power. Defining the power gain (G) as an amplifier's ability to convert RF input power to RF output power, $G = \frac{P_{Out,RF}}{P_{In,RF}}$, equation 4.2 can be rearranged to show the dependence of PAE on efficiency and gain better:

$$PAE = \eta(1 - 1/G). \tag{4.3}$$

It is crucial for PAs to be designed in a way that keeps their efficiency as high as possible while both the power gain and linearity still have acceptable values [72].

4.1.1.2 Linearity

For signals containing both amplitude and phase modulation, linear amplification is important in order to prevent high adjacent channel power and amplitude compression [70, 71]. A linear amplifier can be defined as one that produces an output signal that is a faithful replica of the input signal [72].

4.2 Power Amplifier Classes

The distinction between the various classes of amplifiers happens due to different reasons, such as their circuit configuration, operational topologies, linearity and efficiency. RFPAs are commonly designed as classes A-F [70, 73]. As mentioned earlier, the terms 'linear' and 'nonlinear' are related to the form of the transfer function of the amplifier. Linear amplifiers have three main classes: A, B and A/B, with class A generally being the most linear and least efficient of them all. These types of amplifiers are used where the preservation of the signal is important [74]. The number of nonlinear amplifier classes is more than the linear

ones. These range from self-bias schemes to different forms of switching amplifiers. The main classes for nonlinear amplifiers include classes C, D, E, F, G, H and S. By adopting modified forms of the regular circuit topologies in an attempt to improve the basic efficiency of class B or class C amplifiers, novel configurations were made leading to class F, G and H amplifiers [74].

Amplifier classes determine the proportion of the input cycle (conduction angle) when the current passes through the amplifier. The conduction angle is proportional to the time the amplifier is ON during a full cycle. For example, in a class-A amplifier, the amplifier is always ON during a cycle, therefore, the conduction angle is 360° and in a class-B amplifier, where the amplifier is only ON for half of the cycle, the conduction angle is 180° [75].

FET (Field-Effect Transistor) and BJT (Bipolar Junction Transistor) are both commonly used in amplifier circuits. FETs are voltage-controlled devices, meaning the voltage applied to the gate terminal controls the current flowing through the device. BJTs are current-controlled devices, meaning the current flowing through the device is controlled by the current flowing into the base terminal. Both types of transistors can be used in common-source, common-gate, or common-emitter amplifier configurations. The choice of which type of transistor to use in a particular amplifier circuit depends on the specific requirements of the application, such as voltage and current gain, noise, and input impedance. Both FETs and BJTs can be used to build amplifiers with high power handling capabilities. However, BJTs tend to be more efficient in power handling and are, therefore, more commonly used in high-power applications. On the other hand, FETs are known for their low-noise characteristics and are, therefore, more widely used in low-noise applications. Also, in an amplifier circuit that uses an FET, the gate bias is the DC voltage that is applied to the gate terminal of the transistor

in order to control the flow of current through the device and establish a fixed operating point for the transistor. A positive gate bias will increase the current flow, while a negative bias will decrease it. The gate bias voltage is typically set to a specific value in order to achieve the desired level of amplification in the circuit.

4.2.1 Classic Power Amplifiers

Classic PAs fall into four categories. This includes classes A, B, A/B and C, because of their historical precedence and primarily based on bias conditions. Bias in amplifiers refers to the DC voltage or current applied to the input of a transistor (or other active devices) to establish the operating point, which is also known as the quiescent point. This operating point is established by adjusting the bias conditions so that the device is in its most linear region of operation, where the output signal is a faithful reproduction of the input signal with minimal distortion. The bias conditions determine the amount of current flowing through the device, which in turn affects the overall gain and performance of the amplifier. In classical PAs both the input and output waveforms are considered sinusoidal, which creates some performance and efficiency limitations as it will be discussed later in this chapter [72]. Although class C amplifiers are nonlinear, they use a similar circuit topology to that of class A amplifiers [74]. Figure 4.2 shows a general power amplifier model that can explain the four classical power amplifier classes [72].

In the sketched model shown in figure 4.2, R_L is the load to which the output power is being delivered and *BFL* is a big inductance that feeds DC power to the drain. The *BFL* is assumed to be large enough for the current to be substantially constant. *BFC* is a capacitor that connects the drain to a tank circuit to prevent any possible DC dissipations in the

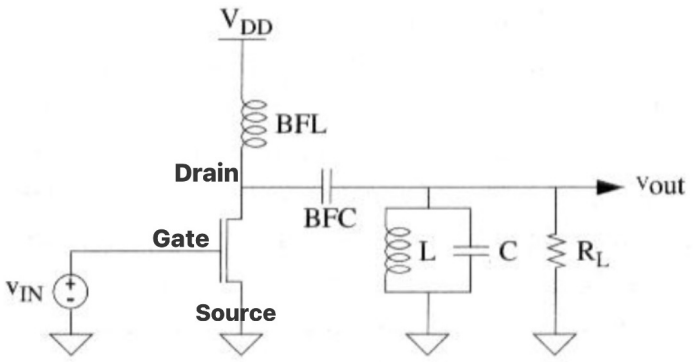

Figure 4.2: A general power amplifier model to understand class A, B, A/B and C amplifiers. *Image and caption reproduced from article [72] with permission (PLSclear reference number: 68997) from publisher: 'Cambridge University Press'.*

load. With this configuration, the transistor's output capacitance can be absorbed into the tank similar to that in small-signal amplifiers. Moreover, the filtering provided by the tank reduces the out-of-band emissions caused by nonlinearities. The discussion here is limited to narrowband PAs and does not cover broadband power amplifiers [72].

4.2.1.1 Class A

In a class A amplifier the operating point and input signal level are chosen so that the output current, collector or drain current, flows at all times. This leads to the power amplifier operating in the linear portion of its characteristic and as a consequence, the signal will face the minimum amount of distortion [74]. It is assumed that the bias levels in a class A amplifier are chosen in a way that the transistor operates linearly [72]. The circuit of an RF class A amplifier is very similar to that of its small signal counterpart. However, the main difference between them is that the signal currents in a power amplifier are a considerable fraction of the bias level and this could translate to potentially serious distortion. But as it can be seen in figure 4.2, in narrowband operation a tank circuit solves the potential

distortion issue associated with such large swings in order to achieve linearity. Since there is always dissipation due to the bias current even with no signals present, the linearity comes at the expense of reduced efficiency [72, 74]. Theoretically, the maximum drain efficiency for a class A amplifier is just 50% and typically, drain efficiencies between 30% to 35% are very common. The calculations leading to these results can be found at [72]. Aside from their low efficiency, class A amplifiers put large amounts of stress on the device. This leads to this type of amplifier rarely being used in RF power applications [72].

4.2.1.2 Class B

One possible way to reduce the transistor dissipation, is to arrange the bias to decrease the fraction of a cycle over which drain voltage and drain current are nonzero at the same time. This is what happens in a class B power amplifier to achieve higher efficiency than a class A counterpart amplifier while still having useful levels of linearity. Figure 4.3 shows the drain voltage and current for an ideal class B PA. In a class B amplifier, the arrangement of the bias is in a way that the output device gets shut off half of every cycle so this type of amplifier only conducts for 50% of the input cycle. The drain efficiency of a class B amplifier is considerably higher than that of a class A amplifier. In class B amplifiers, we have agreed to have some distortion in exchange for a significant improvement in efficiency. Assuming that our components are ideal, the optimum efficiency of a class B amplifier can be calculated as 78.5% [72, 74].

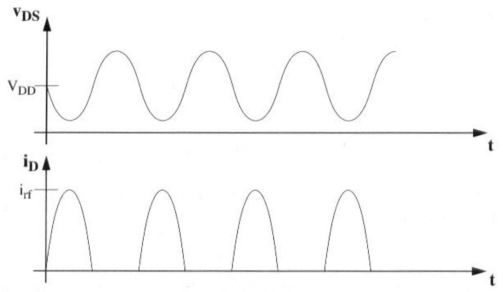

Figure 4.3: The drain voltage and current for an ideal class B amplifier. *Image and caption reproduced from article [72] with permission (PLSclear reference number: 68997) from publisher: 'Cambridge University Press'.*

4.2.1.3 Class A/B

As mentioned before, class A amplifiers conduct 100% of the time and class B amplifiers conduct 50% of the time. A compromise between the two classes A and B leads to a class A/B amplifier. The class A/B amplifier conducts somewhere between 50% and 100% of the time i.e. that the output signal of this type of amplifier is partly zero, where that "part" is less than one-half of the input sinusoidal signal. The chosen bias levels of the amplifier indicate the portion of the time that the amplifier is conducting. The linearity and the efficiency of a class A/B amplifier is intermediate between those of a class A and a class B power amplifier. Class A/B amplifiers add greater distortion than class A amplifiers and less distortion than class B amplifiers. Where the opposite of this is true for the efficiency. The efficiency of a class A/B amplifier is less than a class B stage and more than a class A power amplifier. Good levels of performance can be achieved using this type of PA with only modest levels of standing bias. This makes class A/B amplifiers popular candidates for high RF power amplifier applications [72, 74].

4.2.1.4 Class C

In class C amplifiers, the gate bias is arranged in a way that causes the transistor to conduct less than half of the time, i.e., this type of power amplifier operates somewhere between 0 and 50% of the time. Therefore, the output current (or voltage) of a class C amplifier is zero more than half of an input sinusoidal signal cycle as it can be seen in figure 4.4. As a result, the drain current consists of a periodic train of pulses. Due to the significant distortion of the input signal waveshape, this kind of amplifier is not suitable for linear amplification applications. There are two different types of class C amplifiers: the original or "classical" class C amplifiers which are widely used in MOS amplifiers nowadays, and a more complex type called "class C mixed mode" amplifier that use a BJT [72, 74]. Details about the differences between these two types and more information about their applications can be found at [74].

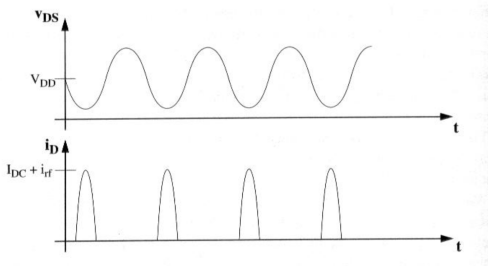

Figure 4.4: The drain voltage and current for an ideal class C amplifier. *Image and caption reproduced from article [72] with permission (PLSclear reference number: 68997) from publisher: 'Cambridge University Press'.*

4.2.2 High Efficiency Power Amplifiers

While the power amplifiers presented so far use the active device as a controlled current source, Class D, E and S amplifiers use the active device as a switch. Therefore their theo-

retical maximum efficiency is 100% with the assumption of the device having zero switching time, no resistance in ON mode and infinite resistance in OFF mode. The reasoning behind using the active device as a switch is that a switch ideally dissipates no power since there is either zero voltage across it or zero current through it. As the product of V-I for the switch is always zero, the transistor dissipates no power and the efficiency has to be 100%. Switched-mode amplifiers such as class D, E or F amplifiers are constant-envelope amplifiers and are not capable of providing an output proportional to the drive. As a result, normally, linear modulation cannot be achieved using this type of amplifier [72, 74].

4.2.2.1 Class D

A class D amplifier can look like a push-pull, transformer-coupled version of a class B amplifier. Figure 4.5 shows a generic diagram of a class D amplifier. As can be seen on the diagram, this amplifier uses a series RLC network in the output instead of the commonly seen parallel tanks. This is because the switch-mode amplifiers are the duals of the current-mode amplifiers that were discussed earlier in this chapter. Consequently, the output filters are also duals of each other. At any given time, only one transistor is driven, with one transistor handling the positive half-cycles and the other the negative ones. This is exactly what happens in a push-pull class B amplifier. However, the transistors here are driven hard enough that it makes them act like switchers rather than as linear amplifiers. This is the main difference between a class D amplifier and the aforementioned class B amplifiers [72, 74].

Since the transistors act as switches, theoretically, the efficiency of a class D amplifier is 100%. This is clearly better than a push-pull class B and a class A amplifier. Figure 4.6 shows the drain voltage and current for an ideal class D amplifier. Although a class D

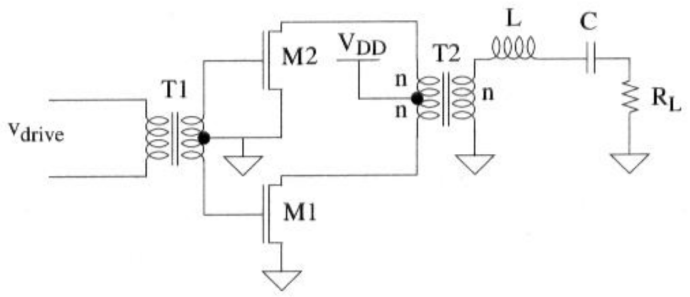

Figure 4.5: A class D amplifier. *Image and caption reproduced from article [72] with permission (PLSclear reference number: 68997) from publisher: 'Cambridge University Press'.*

amplifier cannot normally provide linear modulation, it is capable of providing high efficiency and it does not put much stress on the device.

One of the issues with this type of amplifier is that no perfect switch exists. Due to nonzero saturation voltage, there will always be some static dissipation in the switches and since the switching speeds can be finite, the switch V-I product is nonzero during the transition. Moreover, if one transistor fails to turn completely off before the other one turns on due to charge storage in saturation, a serious reduction in efficiency can result in bipolar implementations. In such a situation, transformer action will attempt to apply the full supply voltage across the device that is not yet off and this can make the V-I product quite large [72].

4.2.2.2 Class E

Although transistors have the potential to enhance efficiency significantly, the associated dissipation with them negatively affects their performance. Thus, to prevent gross losses, it is necessary to have switches that can operate at a high frequency relative to the overall

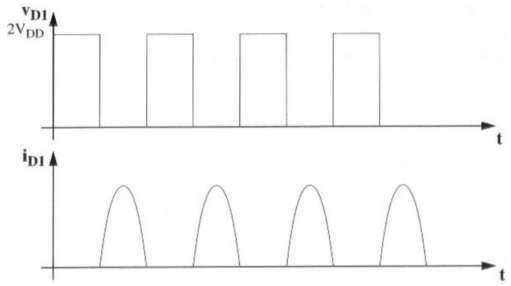

Figure 4.6: Drain voltage and current for an ideal class D amplifier. *Image and caption reproduced from article [72] with permission (PLSclear reference number: 68997) from publisher: 'Cambridge University Press'.*

frequency of operation. Thus, relatively fast switches (relative to the frequency of operation) are required to prevent gross losses. A high-order reactive network is used on class E amplifiers that facilitates enough degree of freedom to shape the switch voltage to have both zero value and zero slope at switch turn-on. This leads to reduced switch losses. Nonetheless, the turn-off transition is often the more troublesome part in bipolar designs and the high-order reactive network does not improve it. Moreover, class E amplifiers cannot handle the power well in spite of their high potential efficiency, which is theoretically 100%, assuming that the switches are ideal. Class E amplifiers are straightforward to design, but due to their poor power capabilities and their reduced efficiency, which is caused by the switch turn-off losses, a practical implementation of them does not show significant superiority to good designs of other types such as a class F amplifier. And since they also require more power, these amplifiers are not very popular or common [72].

4.2.2.3 Class F

The main point of designing class E amplifiers was exploiting the properties of reactive terminations to shape the switch voltage and current waveforms in a way that benefits us. Class F amplifiers follow the same concept more elegently than class E amplifiers. This

type of amplifier's circuit is designed in a way that any frequencies outside of the desired bandwidth will result in a short circuit. With no dissipated power, class F amplifiers can have a theoretical efficiency of 100%, and practically, they can have efficiencies higher than class E amplifiers. Moreover, class F amplifiers have better normalized power-handling capabilities. This type of amplifier is typically used in high-power RF applications, such as in television and radio transmitters since high efficiency is important in these applications in order to minimize heat generation and power consumption.

Class G and class H power amplifiers also exist, but since they can only be used for audio frequency applications and the focus here is on RF power amplifiers, they are not discussed here; more information on these two types of PAs can be found at [74].

4.3 RFPA Performance Metrics

The performance of an RFPA can be examined based on the following timing parameters: PRE, RRT, PFE and RFT. These parameters are defined as [65]:

- PRE: Pulse-to-rising edge time, which is the interval from when the gate pulse is turned on till the beginning of the RF output pulse.
- RRT: RF rise transition time, which is the time that takes the RF output pulse to reach its 100% amplitude.
- PFE: Pulse to falling edge time, which is the time it takes the RF output amplitude to decay once the gate pulse has been turned off.
- RFT: RF fall transition time. This is the delay from when the gating pulse gets turned

if until the RF output turns into noise.

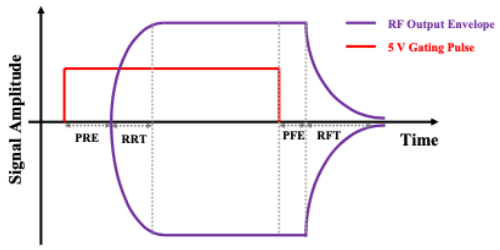

Figure 4.7: RFPA timing parameters and their relations to each other during an RFPA's operation. *Image and caption reproduced from article [65] with permission (license number: 5357820766156) from publisher: 'Springer Nature'.*

4.4 RFPAs For Gradient-free Imaging

Many RFPAs used in MRI parallel transmit (pTX) are usually linear classes such as A, B or A/B, with the first two types having theoretical maximum efficiencies of 50% and 78.5%, respectively. The efficiency of class A/B lies in between these two classes and depends on the conduction angle. Maximum efficiency happens when the output power is at its maximum [72, 76].

4.4.1 Griswold Team Class D Amplifier

There are few amplifier designs that have been used for gradient-free quantitative imaging in the past, one of which is a low-cost modular RFPA platform designed by Dr. Griswold et al [77]. They designed an RFPA for a low-field, gradient-free MRI that uses a method called SENF (Selective Encoding through Nutation and Fingerprinting) [77,78]. A SENF MRI has a B_0 magnetic field of 0.047 T corresponding to 2.07 MHz. This is relatively similar to Merlin's magnetic field and frequency, which are respectively 0.063 T and 2.69 MHz. Their design

includes a compact current mode class D (CMCD) enhancement-mode Gallium Nitride on Silicon (eGaN) FETs RFPA with a high power efficiency [76, 77]. The core of this amplifier includes a 15 mm x 15 mm GaN-based switch-mode PA module (EPC2034c) with 200V drain to source voltage and 48 A continuous drain current.

For designing the output stages of the amplifier, they used simulations of active components from the vendors. "Input modules" produced Transistor-Transistor Logic (TTL) in order to drive the power switching module. An early testing used a simple transistor module that converts external low-amplitude phase-modulated inputs to 50% duty cycle pulses [77].

RFPAs need power cables to carry power to the array of elements. And long RF power cables cause power loss in the array and increase the size and cost of the system [76,79]. These challenges can be addressed by locating the RF power amplifiers on or near the array elements rather than placing them at a remote position. A single shared DC power feed can replace the multiple long RF power cables to considerably increase the power efficiency. Also, small, low-power RF cables can be used. The amplifiers are also able to operate within a strong magnetic field and do not introduce significant B_0 distortion in the imaging volume [76]. To overcome the restrictions of near-coil amplifiers, Heilman et al. [80] proposed using the Current Mode Class D (CMCD) amplifier topology. This allows for higher power density and efficiency than the class A/B RFPAs that are more common [76].

4.4.2 RFPA For TRASE MRI

Initially, class D amplifiers built by LT Imaging (Dr. Logi Vidarsson) were tried on TRASE MRIs. However, due to not achieving reliable imaging, it was decided to switch to class A/B amplifiers to reduce the number of unknowns in the electronics chain. A gain of at least

+50 dB was required in order to achieve a desired output power of 100 W directly from an input power of 10 mW. Dr. Vidarsson's design was an on-coil FET-based class D amplifier that was fairly efficient and produced square waves as expected of class D amplifiers. In the beginning, a class D RFPA seemed like the best design for TRASE-based MRIs. This was because our portable prototypes of MRI are designed for use in International Space Station (ISS), and due to power limitation of ISS, amplifiers similar to a class D were the best options. Additionally, the decoupling features of an FET amplifier could possibly eliminate the need for power-consuming PIN diodes needed for switching. Besides, theoretically, class D amplifiers can have a 100% efficiency. However, the on-coil class D amplifier had safety issues. Unfortunately, if it overheated, it could burn an astronaut, and as a result, a more traditional class D amplifier was chosen instead of an FET-based amplifier.

The class D amplifier built by the LT Imaging employed two high power FETs in a push-pull configuration and it produced a spin-echo sequence at the Merlin frequency. Nevertheless, due to the class D amplifiers not being able to generate reliable RF pulses for output powers of below 20 W (desirable output power was 1W), specifying pulse heights with higher precision was not possible and having enough control over the RF output was not achievable. The class D amplifier technology is quite novel and in order for it to be used in TRASE applications, it needs to be better understood. Besides, as it was mentioned before, this type of amplifier is nonlinear. So, the RF pulses it generates are not made of clear and decent sinusoids. As a result, it was decided to switch to using class A/B amplifiers in hope of having more accurate control over the output power and better waveforms.

Four AN779H-12 20 W high-gain, high-frequency class A/B amplifiers were initially tried with the Merlin MRI, which originally had a four-channel RF transmit chain. This amplifier

design uses a 12V DC input power and provides an output RF power of ∼20 W with a typical RF power gain of ∼+50 dB. The Owl MRI's modified two-channel RF transmit system used two of these RFPAs. Although these class A/B amplifiers were linear, they produced more noise than class D amplifiers. This lead to an effort by myself to build a blanking circuit for the amplifiers. I followed Dr. Vidarsson's design in building a diode-based blanking circuit that could turn-off the transmit amplifier during receive. Figure 4.8 shows blanking circuit diagrams with one, two and three diode stages. With increasing the number of diodes, the noise reduces and the distortion increases. Figure 4.9 shows the blanking circuits that were built based on Dr. Vidarsson's design. Nevertheless, the work on the blanking circuits stopped because one of the amplifiers failed. Therefore, it was decided to switch to a different design. I built part of a class A/B amplifier with built-in blanking designed by Dr. Aaron Purchase, a collaborator at the university of Alberta. The amplifier was modified to work with TRASE MRIs and is discussed further in this chapter [32].

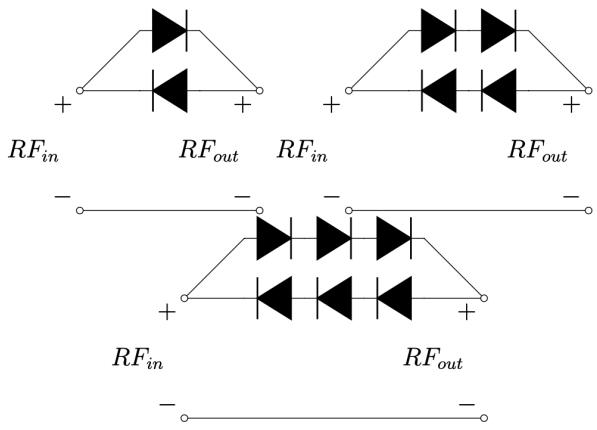

Figure 4.8: Diagrams for three variants of the diode-based blanking circuit. Top left shows a single stage diode circuit, top right shows a two stage diode circuit, and at the bottom there is a three stage diode circuit. *Image credit goes to Dr. Logi Vidarsson - under Fair Dealing Exception permission [29]*

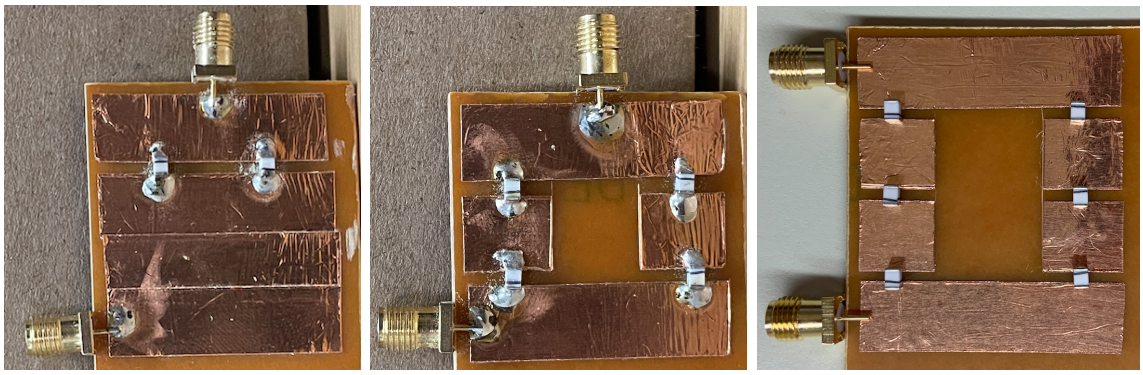

Figure 4.9: Three variants of the diode-based blanking circuit. From left to right, one-stage, two-stage and three-stage blanking circuits. *Images taken by the author*

In order to have the maximal TRASE MR image resolution, high-power RF output ($\geq 1kW$), high duty cycle ($\geq 50\%$), and fast switching times ($\leq 10\mu s$ PRE and PFE; $< 5\mu s$ RFT and RRT) are required. Additionally, as it was briefly discussed earlier, blanking is necessary to minimize the RF output noise [65].

Characteristic	Requirement
Class	A/B
Peak RF power output	$\geq 1kW$
RF duty cycle	$\geq 50\%$
BNL (Blanked Noise Level)	$\leq -171dBm/Hz$
PRE & PFE (Pulse-to-Rising/Falling Edge)	$\leq 10\mu s$
RRT & RFT (RF Rise/Fall Transition Times)	$\leq 5\mu s$
Minimum pulse length	$\leq 100\mu s$
Harmonics strength at 1 kW	$< -12dBc$
Number of channels	≥ 2
Total gain	+ 60 dB

Table 4.1: Requirements for a 1D TRASE MRI RFPA. *Table and caption reproduced from article [65] with permission (license number: 5357820766156) from publisher: 'Springer Nature'.*

4.5 Origin of the RF Amplifier Design

Reasons as to why a specific type of high-power RF amplifier is needed for TRASE MRI were mentioned earlier. Here, the process of constructing the RFPA designed to be used on the Merlin MRI is discussed. The initial design of this amplifier was by Jim Klitzing in California on Amateur Radio Station W6PQL website [81, 82]. Dr. Aaron Purchase from the University of Alberta, where other teams are working on TRASE MRI, made some modifications to the RFPA design from the W6PQL website to make it compatible with TRASE MRIs. He also added a switching gating circuit to the main design to help with the duty cycle requirements [65]. Following the instructions on the W6PQL website and Dr. Purchase's paper on his design, this RFPA was reassembled as part of this work to be used with the Merlin MRI. These RFPAs have also been used and are being used with the 0.2 T MRI-Tech MRI and with Dr. Purchase's IRIS MRI. [32]

4.6 Assembly and Parts

The assembly of the RFPA was based on the instructions given on the W6PQL website. To test the device, a testing procedure was also given on the website. The changes based on Dr. Purchase's design were supposed to be applied later on, after the testing was completed. Therefore, the images of the RFPA included in this chapter will be based on the schematic given in figure 4.10.

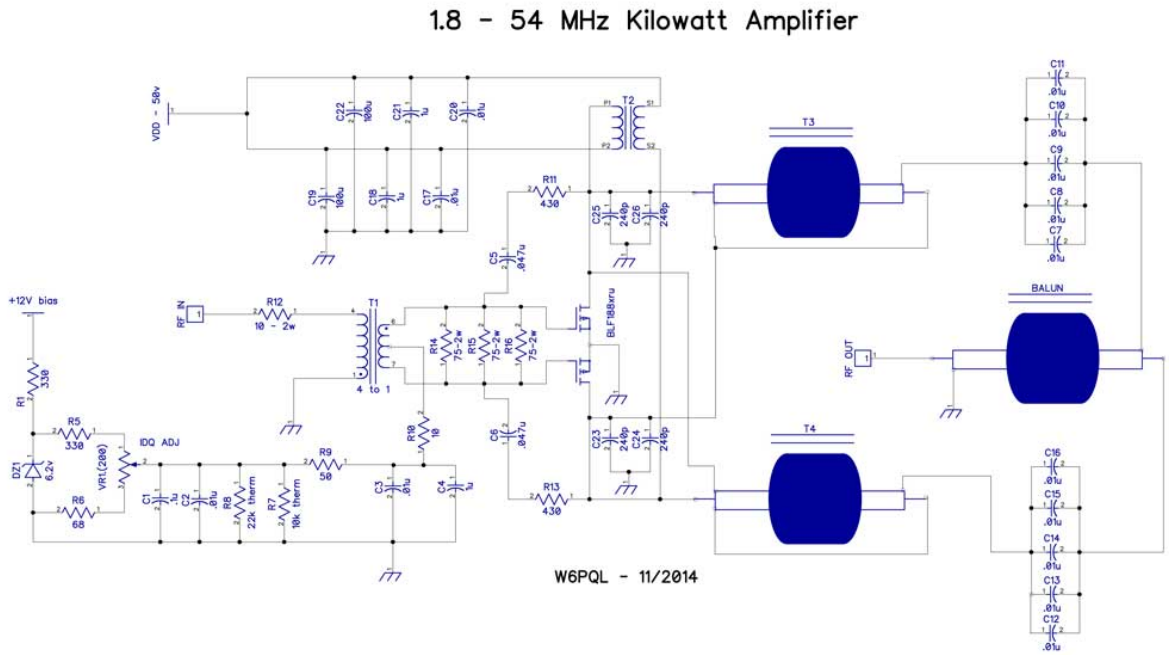

Figure 4.10: The main schematic of the RFPA designed by Jim Klitzing. *Images taken from [83], Copyright permission granted by Mr. Kim through email.*

4.6.1 Components

The main parts that were used for this assembly and its testing are listed below:

- The main RFPA deck [82].
- A 50 V power supply used to power the main RFPA. (GOPHERT NPS-1602)
- A 12 V power supply to power the bias. (Here, the same 50 V power supply was used to provide the 12 V, as well.)
- A pre-amplifier to amplify the signal before sending to the main RF deck. (Mini-Circuits ZHL-32A+)
- A 24 V power supply for powering the pre-amplifier. (Advantech PWR-242-AE)

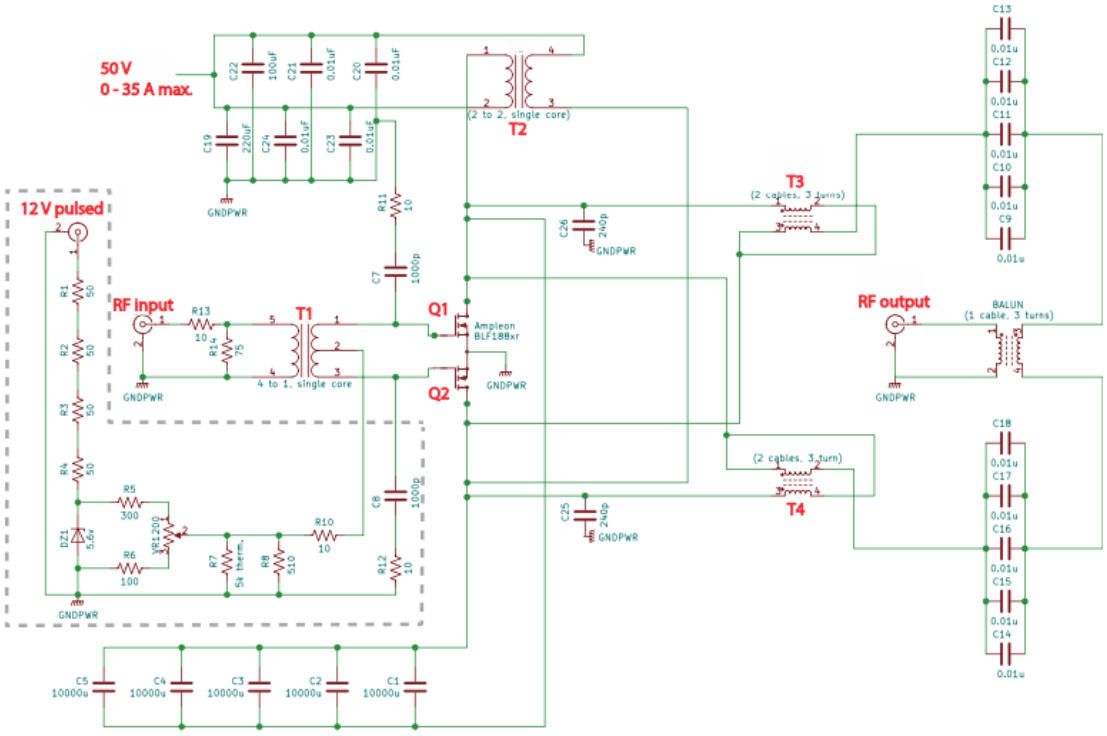

Figure 4.11: Schematic of the RFPA after Dr. Purchase's modifications. *Image and caption reproduced from article [65] with permission (license number: 5357820766156) from publisher: 'Springer Nature'.*

- USB Oscilloscope and Logic Analyzer Analog Discovery 2 (Digilent AD2) and the Owl SDR (Software-defined-radio) for signal generation.

- An oscilloscope for measuring the output signal. (Tektronix TDS 2024C (200 MHz – 4 channel oscilloscope with a $1M\Omega$ impedance))

Since Mr. Jim Klitzing designed this amplifier to be used in amateur radio broadcasting, it does not take into consideration the requirements of an RFPA used for MRI applications. In MR imaging, noise needs to be at a minimal level and multiple, high-power signals need to be sent. This means the continuous wave mode (CW) used in radio communications needed to be replaced with pulsed mode for signals [65].

To fulfill this purpose, Dr. Purchase designed a blanking circuit for the W6PQL amplifier

by converting a 12 V DC power input to a 12 V pulsed signal. A schematic of this design can be seen in figure 4.18. To generate 12 V gating pulses, a gating controller was constructed.

The main RF amplifier design consists of five circuits. The RF input which receives the signal from the pre-amplifier, the bias network, the main power supply, which sends 50 V to the transistors, transistors circuit and the RF output [65].

Dr. Purchase removed R7 and R8 resistors in figure 4.10 from the circuit in order to reduce PRE and PFE delays caused by RC integrating effect. The TC-18 Teflon coax also was not included on the amplifier he built. According to the W6PQL website, this is only required for the 6M band, which is the 50 MHz range. And since the frequency that we use for the Merlin MRI is as low as 2.69 MHz, it is not necessary for us to include that on our RFPAs.

While making modifications to the main power supply circuit, Dr. Purchase also included five additional capacitors ($C_1 - C_5$ 10 mF each with parallel connections to each other, figure 4.10). This was to decrease the transient response time of the power supply during pulsed operation. These extra capacitors can be charged and discharged faster than the main power supply can get turned on and off. Therefore, they provide a more easily accessible power source [65]. During the blanking period, the capacitors were charged and they were quickly discharged during the transmission period. They were not necessary for the RFPA, however, they were useful additions that could minimize any problems from the VDD while the RFPA was not on the testing stage anymore and was ready to be used with the Merlin.

4.6.2 Pre-Amplifier

To achieve a +60 dB gain, a two-stage design was selected where a pre-amplifier was used in the first stage to amplify a 2.69 MHz (10-60 mV) RF input signal. The ZHL-32A+ amplifier built by Mini-Circuits ZHL-32A+ is a class-A amplifier with high RF output linearity. It was selected due to its reliability, small dimensions (3.75″ x 2.60″ x 1.80″) and the proper amount of gain it is able to provide. Based on its data sheet, this pre-amplifier has a +27 dB gain at 2.69 MHz, which is the frequency we use based on the Merlin MRI's needs. This pre-amplifier was powered by a 2.1 A, 24 V, Advantech PWR-242-AE power supply.

Even during the testing process of the main RFPA, the pre-amplifier was needed. Because the RFPA transistors have specific signal requirements and under-powering them results in their malfunction. Also, a 30 dB dummy load (50 Ω attenuator) was used at all times, therefore, some gain from the pre-amplifier was necessary.

Input RF Signal Amplitude (mV)	Output RF Signal Amplitude (mV)	Gain (dB)
10	180	25.10
20	340	24.61
30	500	24.44
40	650	24.22
50	800	24.08
60	970	24.17

Table 4.2: Pre-amplifier gain measurements.

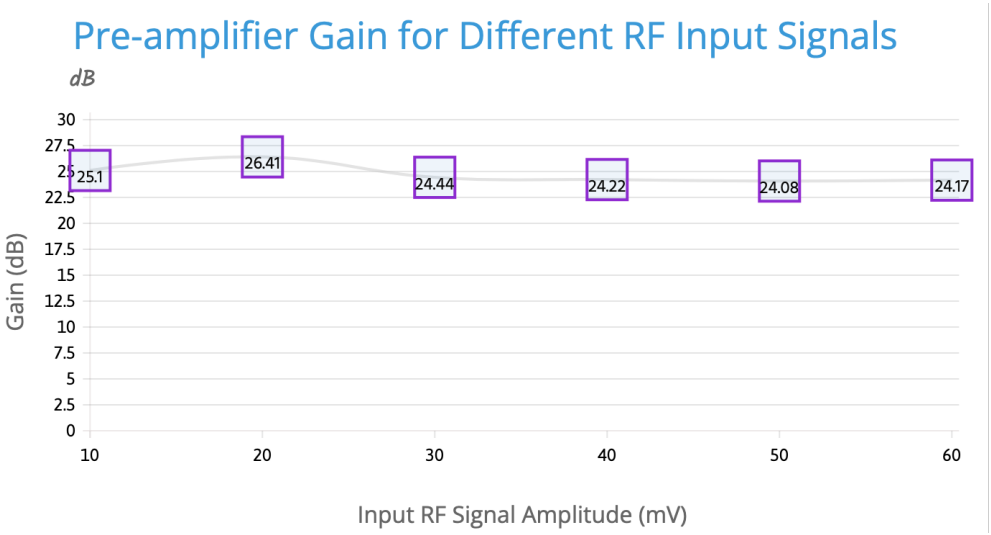

Figure 4.12: Pre-amplifier gain graph for different RF inputs.

To test the pre-amplifier, RF signals were generated using the AD2 SDR, the pre-amp was powered using the 12 V DC power supply and the output was connected to the oscilloscope for measurements. All connectors used for any experiments in this project were 50Ω coaxial cables with SMA connectors (at some cases BNC to SMA connectors were used such as for connections to AD2). Based on the measurements, this pre-amplifier has an average of +24.44 dB gain for a signal with a 2.69 MHz frequency in the range of 10-60 mV.

4.6.3 Input Signals

Analog Discovery Channel 2 (AD2) was the main source of signal generation used for testing the amplifiers after assembly. It is capable of generating clear continuous sinusoidal signals with desirable frequency. However, Dr. Logi Vidarsson (LT Imaging) wrote a Free Induction Decay (FID) pulse sequence as part of the Owl MRI software, which was an RF pulse followed by a data acquisition window. This FID pulse sequence was intended to be used for necessary flip-angle adjustments before any NMR experiments. It generated the most basic pulse

sequences for testing and defining the RFPA characteristics, such as RF power gain. Also, it was tested itself on an oscilloscope to make sure of the accuracy of the pulse sequence it was capable of generating. Since the pulse sequence that is used for TRASE imaging is generated by this SDR, the gain measurements were also done with signals generated by this SDR and the results for the amplifier gains were similar to what is shown in table 4.3.

4.6.4 Main Deck

As mentioned before, the main RFPA deck was designed by Jim Klitzing on W6PQL website [82]. The list of the Bill of Materials (BOM) that are used to assemble this deck can be found on [83]. This deck contains a power transistor (BLF188XR Transistor) with an average gain of +25 dB. This RFPA is compact and has a size of 4″ x 6.5″ and uses Arlon TC-350 for its PC board material with a high thermal conductivity that draws the heat away from the components [83].

The LDMOS (BLF transistors) came flow-soldered to a 3″ x 5″ x 1/2″ copper heat spreader, which helps dissipate the heat that is generated at high power. The spreader also needs to be secured to a heat sink with machine screws and thermal paste. These should be used at the joint to take the heat further away, so that fans could move the heat outside the amplifier enclosure. 1/2 ″ spacers needed to be used around the edges of the spreader so the board does not overhang the copper [83]. This was the design because this amplifier was originally used for CW at 1 kW and the transistors dissipate quite a bit of heat at these high powers with continuous wave. Nevertheless, initially we decided that the aluminum heat sink was not necessary since our power requirements are comparably low. Therefore, not much heat was expected to be generated that needed removal. This was the assumption,

however, since the gating circuit was not included, a heat sink became necessary even for testing. Cooling fans were used instead for heat removal, but it was decided to include the heat sink.

4.6.4.1 Assembling the Main RFPA

The RFPA deck was assembled following the instructions on the W6PQL website [82]. This process included building and installing the transformers and soldering them on the output board with the rest of the components and assembling the input board.

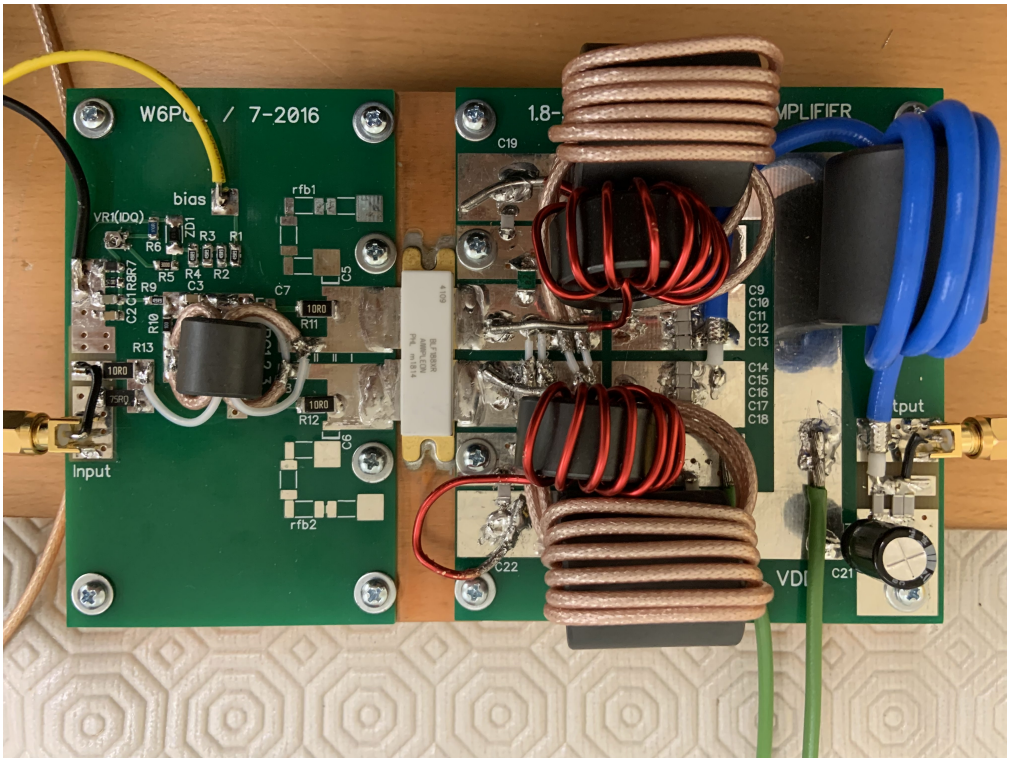

Figure 4.13: The main RFPA deck after assembly.

After the assembly was complete, the main amplifier was tested. Figure 4.17 shows the setup for testing the amplifiers. The power supply provided 50 V VDD and 12 V bias for the RFPA. The signals were generated by the AD2 SDR and sent to the pre-amplifier through

50Ω coaxial cables for amplification. The output of the pre-amplifier was connected to the input of the main RFPA. The idling current drawn by the LDMOS on the RFPA (IDQ) was adjusted for 2 A and the output of the RFPA was connected to one of the channels on the Tektronix oscilloscope. The expected gain from this RFPA based on the BLF188XR transistor's data sheet was +29 dB. However, what was being measured initially was not the expected gain. After running more tests on the set up such as checking the components, and replacing some of them (because of the way they were added to the circuit, a multimeter could not test them properly), trying different lead for soldering, etc., it was found that there was a cold solder with one of the components. After re-soldering, the connections and the performance of the RFPA improved. However, the gain was still lower than what was expected. It was then discovered that a Zener Diode was malfunctioning and replacing it resolved the problem. Other parts of the deck were also tested to make sure that everything was working properly. During these tests, the bias voltage was always 12.22 V and the IDQ was adjusted to 2 Amps. Since the Merlin requires two of these RFPAs, the second one was also assembled and the results for each of their gains is given on the table 4.2.

As we know from RF design basics, the voltage gain (V_{out}/V_{in}), and the power gain (P_{out}/P_{in}) are expressed in decibels (dB) and can be derived using the following equations [70]:

$$A_V|_{dB} = 20 \log \frac{V_{out}}{V_{in}} \tag{4.4}$$

$$A_P|_{dB} = 10 \log \frac{P_{out}}{P_{in}}. \tag{4.5}$$

If and only if the input and output voltages appear across equal impedances, these two

quantities are equal in dB:

$$A_P|_{dB} = 10 \log \frac{\frac{V_{out}^2}{R_0}}{\frac{V_{in}^2}{R_0}} \tag{4.6}$$

$$= 20 \log \frac{V_{out}}{V_{in}} \tag{4.7}$$

$$= A_V|_{dB}, \tag{4.8}$$

where V_{out} and V_{in} are rms values. Since the impedance matching was done for the input and output signals (R_0 is 50Ω), input and output voltages were used to do the gain calculations.

Input RF Signal Amplitude (V)	0.01	0.02	0.03	0.04	0.05	0.06
Pre-amplifier Output RF Signal Amplitude (V)	0.18	0.34	0.50	0.65	0.80	0.97
Pre-amplifier Gain (dB)	25.10	24.61	24.44	24.22	24.08	24.17
RFPA1 Output Signal Amplitude (V)	5.1	10.0	14.2	18.5	22.3	25.6
RFPA1 Gain (dB)	29.05	29.37	29.07	29.08	28.90	28.43
RFPA2 Output Signal Amplitude (V)	5.4	10.1	14.6	18.8	22.3	25.8
RFPA2 Gain (dB)	29.54	29.46	29.31	29.22	28.90	28.50

Table 4.3: Pre-amplifier and RFPAs' gain measurements. RFPA gain measurements are done with the signal going through a 30 dB attenuator attached to the the oscilloscope. A 50 Ω BW-S30W20+ attenuator from Mini-Circuits with SMA connectors is used for this purpose (The attenuator does not affect the numbers in the RF output rows, numbers in those rows have been increased by +30 dB to make it easier to compare). The amplitudes and measurements stated in this table are all based on using AD2. The RFPAs can generate $\sim$ 1 kW output for 3 mW of input RF power.

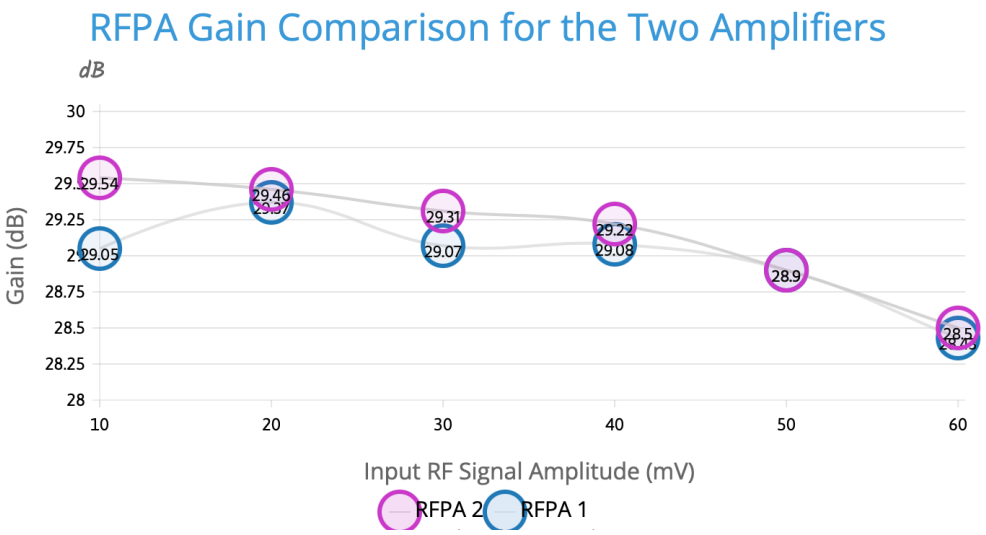

Figure 4.14: Gain comparison between the two amplifiers after assembly.

In figure 4.15 a sinusoidal RF signal which is the output of one of the RFPAs can be

seen. The input signal used to generate this output is a 30 mV RF signal that has been amplified in two stages - first through the pre-amplifier and then through the main deck. The output voltage of this signal is 17.6 V, which corresponds to a total gain of 55.37 dB. The pre-amplifier has a gain of 24.44 dB for a 30 mV input signal, so the main amplifier in this image has a gain of approximately +30 dB. Figure 4.16 shows a block diagram of the how the pre-amplifier, power supplies and the gating controller are connected together and figure 4.17 shows the testing setup of the amplifier.

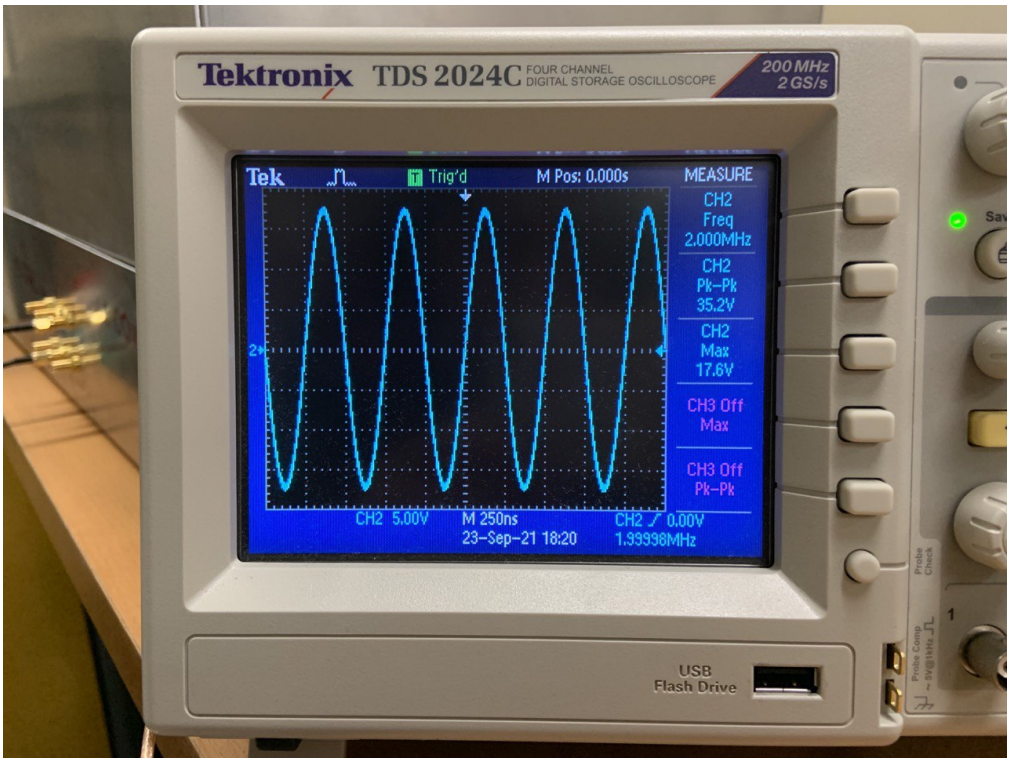

Figure 4.15: The output signal for one of the RFPAs.

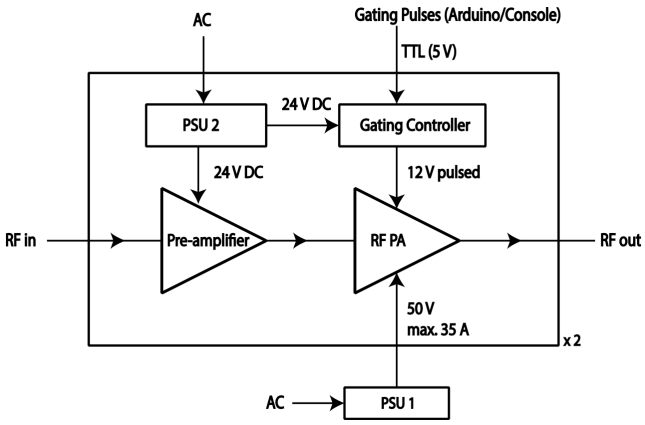

Figure 4.16: A block diagram showing how the pre-amplifier, power supplies and the gating controller are connected together. *Image and caption reproduced from article [65] with permission (license number: 5357820766156) from publisher: 'Springer Nature'.*

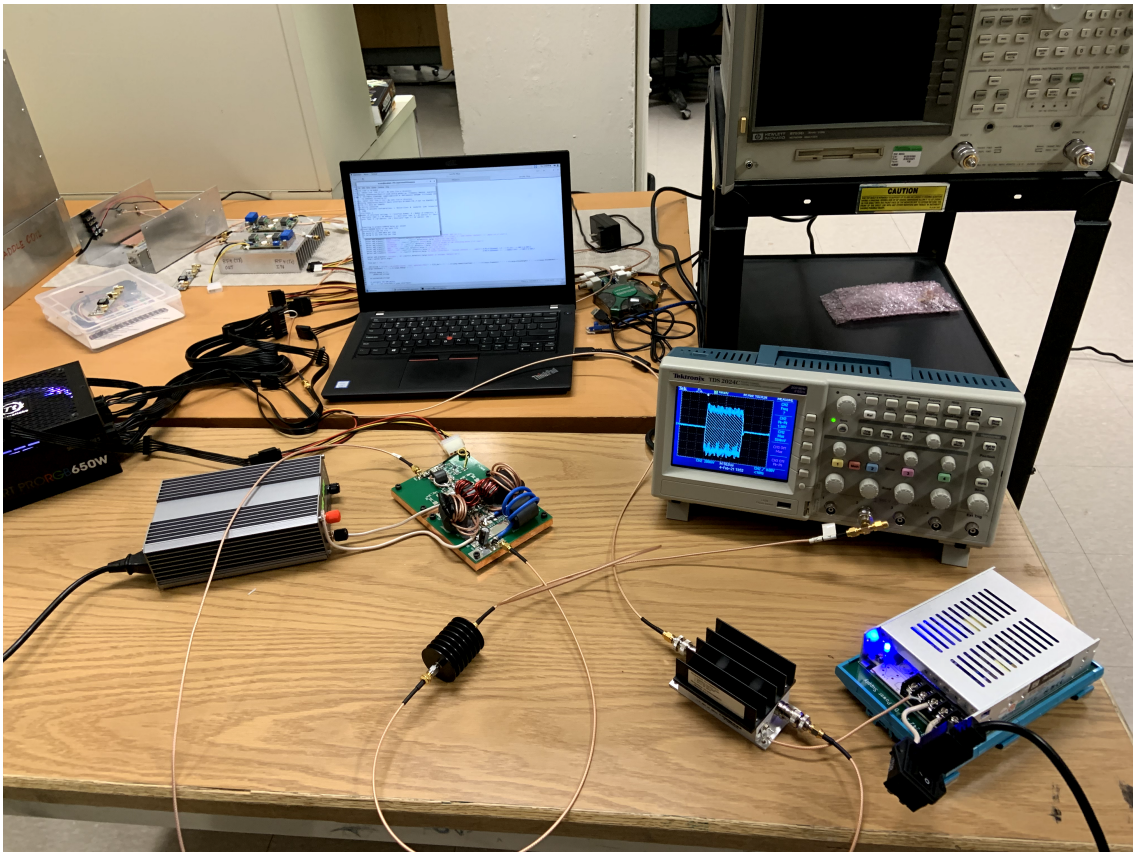

Figure 4.17: The set up used for testing the amplifiers. At the left side of the picture, there is the power supply that provides the 12 V needed for bias. The grey power supply is the main PSU needed for the main deck that gives 50 V DC. The Owl computer which is a ThinkPad is connected to AD2 (the green square-shaped box at the right side of the laptop) and the signal generated by AD2 or the FID pulse sequence can be sent to the pre-amplifier. That is the small black amplifier in the front, which is powered by the grey and blue PSU besides it and provides 24 V. The signal then goes through the main deck with transformers on it. After going through an attenuator, the signal then goes into an oscilloscope.

4.6.5 Gating Circuit

Pulsing the 12 V bias voltage that goes on the RFPA, and therefore, switching the signal to ON/OFF allows noise blanking and reduces electronic noise during signal acquisition. A gating circuit was assembled following the design by Dr. Purchase on figure 4.18. In the initial tests, the voltages I was testing on the circuit seemed correct. The pulsing gate was converting 24 V DC to 12 V DC and then 5 V DC. The AD2 was capable of generating a 5V pulsed signal. Nevertheless, as the 5V pulsed signal was being sent on the input side of the board, a pulsed 12V signal was not being received at the output, which was connected to the oscilloscope. Instead of 5 V, 2 V was being measured on the circuit. Eventually, I ran out of time before I could finish assembling the gating circuit and troubleshoot it. However, figure 4.19 shows the gating circuit that was assembled. Figure 4.18 shows a schematic of Dr. Purchase's gating controller.

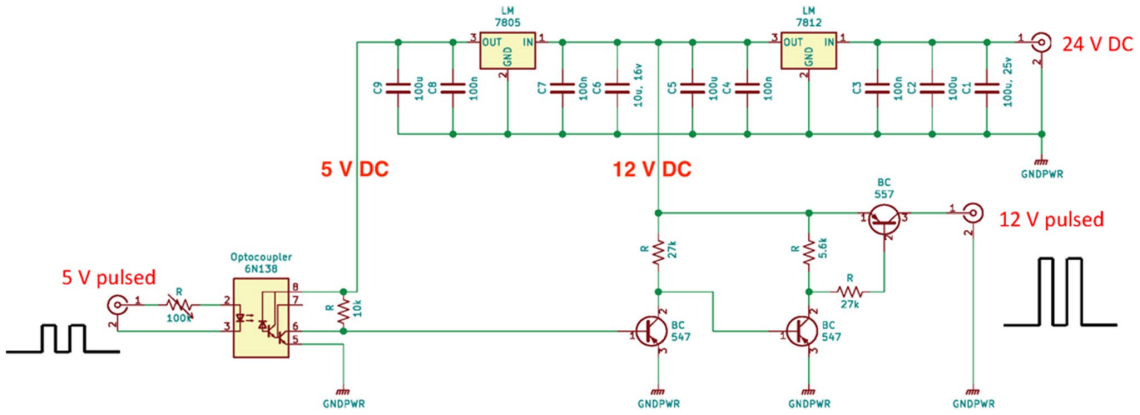

Figure 4.18: Schematic of Dr. Purchase's gating controller circuit. *Image and caption reproduced from article [65] with permission (license number: 5357820766156) from publisher: 'Springer Nature'.*

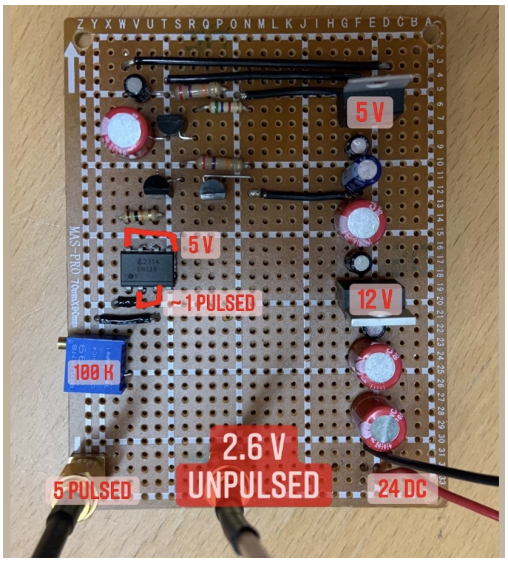

Figure 4.19: The assembled gating circuit for pulsing the 12 V bias voltage.

4.6.6 Thermal Concerns

BLF188XR transistors that are used in the assembled amplifiers are normally used with CW. Therefore one might expect pulsing the power to not affect the heat generation process. Nevertheless, these decks are used in Amateur Ratio and they are not designed to switch on and off really fast in that application whereas we must turn the transistors off to measure the NMR in our systems, which causes more heat to be generated. Gating or disabling the RFPA output stage while the signal is being acquired reduces electronic noise and this is important in order to maximize SNR in MRI application. When the gate is on in CW, even without any RF signal input, heat gets generated. When transistors are turned OFF, they act like resistors and the power (idling) from the power supply is dissipated.

During the testing stage of the RFPA, although the gating circuit had not been built at that time and the amplifiers were not operating in pulsed mode, it was noted that there was some heat being generated by the RFPAs, when they had been turned on for a while. These

amplifiers need aluminum heat sinks for heat dissipation and since the aluminum heat sinks were not added to the setup yet, the generated heat was affecting the current drawn by the IDQ and causing issues with the testing, therefore cooling fans were added. Using cooling fans made it possible to perform examinations on the RFPAs, since the fans could dissipate the generated heat.

5 Conclusion

In this thesis, the primary objective was to learn about recent advancements in portable, low-field MRI and to contribute to this field of technology by constructing the RF power amplifiers required for the TRASE MRIs. Some other electronic parts including multiple-staged blanking circuits and a gating circuit were also constructed in the process of this research.

In Chapter 2, the most significant portable MRI technologies are briefly discussed. Most of the portable devices outlined here are low field MRIs with the exception of a couple of them having slightly higher magnetic fields and falling into the category of mid field MRIs. Some of these devices are only experimental while others have already gone through the experimental stages and are commercially available. For example, Hyperfine and MR Cap are both low field MRIs with a field strength of 0.064 T and are designed for brain imaging; however, while MR Cap would need to overcome several practical requirements before it could be used for POC applications, Hyperfine has received clearance from FDA and is commercially available. There are other pMRIs that were approved by FDA such as The Applause by MagneVu and Promaxo. MagneVu went out of business in 2007, but Promaxo, which is an office-based prostate scanner, was just FDA cleared in 2021 and is operating. Although most of the MRI scanners built around the world are aimed for diagnostic applications in humans, there are also a few devices that are meant for applications other than human health monitoring such

as investigating arbitrary objects and studying plants. The NMR MOUSE and The Tree Hugger are examples of such devices.

B_0 gradient field coils are essential parts of traditional MRIs and eliminating them leads to gradient-free imaging methods, one of which is TRASE. TRASE uses RF gradients for spatial encoding, which can improve the compactness and mobility of the MRI scanners since traditional gradient coils are normally large and heavy components. Eliminating the gradient coils also removes the noise and the need for gradient coil amplifiers. While conventional MRI scanners use high field superconducting permanent magnets that can weigh up to 10 tons, TRASE MRIs use light-weight low-field permanent magnets. Both conventional and TRASE MRIs need amplifiers to amplify the transmit signal before sending it. Conventional MRI scanners can use commercially available RFPAs, however, TRASE has specific requirements such as high duty-cycle. Therefore, TRASE needs specific RFPAs.

Since some TRASE-based prototypes of MRI such as the Merlin and the Owl are being developed at Usask, there was a need for building specific TRASE amplifiers. The focus of this work in the Space MRI Lab was constructing the required TRASE RFPAs. The initial design of this amplifier was done by Jim Klitzing in California on Amateur Radio Station W6PQL website and Dr. Aaron Purchase modified it be more compatible with TRASE MRIs. The amplifier was a two-stage, class A/B, push-pull RFPA constructed to work with the Merlin, an ankle-sized, TRASE MRI (63 mT) built in Dr. Sarty's Space MRI Lab. Since Merlin is meant to be put in ISS for astronaut health monitoring, a class D amplifier seemed like a good candidate due to its high efficiency and the ISS power limitations. Nevertheless, because of technical difficulties associated with a class D RFPA, it was decided to proceed with a class A/B amplifier for the time being. After the assembly, both of the RFPAs

were tested and measurements were obtained from the tests. Fortunately, they both showed desirable results and can now be used to replace our old RFPAs to improve the SNR and acquire images with better qualities. The RFPAs have a high duty cycle which is 50% at its minimum and are capable of providing +60 dB amplification and up to 1 kW RF output. As the work on TRASE continues at the Usask and the U of A to improve the TRASE technique and as more TRASE MRIs are being built and tested, these RFPAs seem to have proven to be suitable components in the setup. If the future TRASE designs require an RF output power higher than 1 kW, available high-power combiner circuits could be included with the RFPAs.

Bibliography

[1] P. Sprawls, *magnetic resonance imaging*. [Online]. Available: https://www.google.com/search?client=safari&rls=en&q=magnetic+resonance+imaging+textbook+pdf&ie=UTF-8&oe=UTF-8

[2] G. E. Sarty, "Introduction to Magnetic Resonance Imaging," p. 205.

[3] "Novel MRI technology will monitor astronauts' health in space." [Online]. Available: https://news.usask.ca/articles/research/2018/novel-mri-technology-will-monitor-astronauts-health-----.php

[4] "Mini MRI to check bone health on space station." [Online]. Available: https://www.newscientist.com/article/dn26385-mini-mri-to-check-bone-health-on-space-station/

[5] "Portable MRI machine opens a world of possibilities for M Health Fairview patients." [Online]. Available: https://mhealthfairview.org/blog/m-health-fairview-trials-portable-magnetic-resonance-imaging-mri-machine

[6] A. Galante, N. Catallo, P. Sebastiani, A. Sotgiu, R. Sinibaldi, C. De Luca, A. Conti, V. Pizzella, G. Romani, and S. Della Penna, "Very Low Field MRI: A fast system compatible with Magnetoencephalography," in *2015 IEEE International Symposium on Medical Measurements and Applications (MeMeA) Proceedings*, May 2015, pp. 560–564.

[7] M. Sarracanie and N. Salameh, "Low-Field MRI: How Low Can We Go? A Fresh View on an Old Debate," *Frontiers in Physics*, vol. 8, 2020. [Online]. Available: https://www.frontiersin.org/article/10.3389/fphy.2020.00172

[8] M. H. Mazurek, B. A. Cahn, M. M. Yuen, A. M. Prabhat, I. R. Chavva, J. T. Shah, A. L. Crawford, E. B. Welch, J. Rothberg, L. Sacolick, M. Poole, C. Wira, C. C. Matouk, A. Ward, N. Timario, A. Leasure, R. Beekman, T. J. Peng, J. Witsch, J. P. Antonios, G. J. Falcone, K. T. Gobeske, N. Petersen, J. Schindler, L. Sansing, E. J. Gilmore, D. Y. Hwang, J. A. Kim, A. Malhotra, G. Sze, M. S. Rosen, W. T. Kimberly, and K. N. Sheth, "Portable, bedside, low-field magnetic resonance imaging for evaluation of intracerebral hemorrhage," *Nature Communications*, vol. 12, no. 1, p. 5119, Dec. 2021. [Online]. Available: https://www.nature.com/articles/s41467-021-25441-6

[9] "Hyperfine's Swoop Portable MRI System." [Online]. Available: https://www.medicaldevice-network.com/projects/hyperfines-swoop-portable-mri/

[10] "Easy to Use, Bedside MRI: About Swoop® Portable MR Imaging System™." [Online]. Available: https://hyperfine.io/product/

[11] "Hyperfine Receives FDA Clearance for Portable MRI Technology - ProQuest." [Online]. Available: https://www.proquest.com/openview/5c609d9987037cd3e2d4e866bfbc9ad0/1?pq-origsite=gscholar&cbl=2037571

[12] "JFK University Medical Center First Hospital in New Jersey to Utilize New Portable MRI - ProQuest." [Online]. Available: https://www.proquest.com/openview/bf15d7a723e226600c15c219eb7ae72f/1?pq-origsite=gscholar&cbl=2037571

[13] "Study Published in JAMA Neurology Confirms Low-Field MR Imaging Using Hyperfine's Swoop™ Portable MRI Successfully Detects Abnormalities at Bedside of Critically-Ill Patients," Sep. 2020. [Online]. Available: https://hyperfine.io/study-published-in-jama-neurology-confirms-low-field-mr-imaging-using-hyperfines-sw\oop-portable-mri-successfully-detects-abnormalities-at-bedside-of-critically-ill-patients/

[14] M. H. Mazurek, B. A. Cahn, M. M. Yuen, A. M. Prabhat, I. R. Chavva, J. T. Shah, A. L. Crawford, E. B. Welch, J. Rothberg, L. Sacolick, M. Poole, C. Wira, C. C. Matouk, A. Ward, N. Timario, A. Leasure, R. Beekman, T. J. Peng, J. Witsch, J. P. Antonios, G. J. Falcone, K. T. Gobeske, N. Petersen, J. Schindler, L. Sansing, E. J. Gilmore, D. Y. Hwang, J. A. Kim, A. Malhotra, G. Sze, M. S. Rosen, W. T. Kimberly, and K. N. Sheth, "Portable, bedside, low-field magnetic resonance imaging for evaluation of intracerebral hemorrhage," *Nature Communications*, vol. 12, no. 1, p. 5119, Aug. 2021, number: 1 Publisher: Nature Publishing Group. [Online]. Available: https://www.nature.com/articles/s41467-021-25441-6

[15] P. C. McDaniel, C. Z. Cooley, J. P. Stockmann, and L. L. Wald, "The MR Cap: A single-sided MRI system designed for potential point-of-care limited field-of-view brain imaging," *Magnetic Resonance in Medicine*, vol. 82, no. 5, 2019. [Online]. Available: https://onlinelibrary.wiley.com/doi/abs/10.1002/mrm.27861

[16] M. Nakagomi, M. Kajiwara, J. Matsuzaki, K. Tanabe, S. Hoshiai, Y. Okamoto, and Y. Terada, "Development of a small car-mounted magnetic resonance imaging system for human elbows using a 0.2 T permanent magnet," *Journal of Magnetic Resonance*, vol. 304, pp. 1–6, Jul. 2019. [Online]. Available: https://linkinghub.elsevier.com/retrieve/pii/S1090780719300837

[17] L. L. Wald, P. C. McDaniel, T. Witzel, J. P. Stockmann, and C. Z. Cooley, "Low-cost and portable MRI," *Journal of Magnetic Resonance Imaging*, vol. 52, no. 3, pp. 686–696, Sep. 2020, publisher: John Wiley & Sons, Ltd. [Online]. Available: https://onlinelibrary-wiley-com.cyber.usask.ca/doi/10.1002/jmri.26942

[18] C. Z. Cooley, J. P. Stockmann, B. D. Armstrong, M. Sarracanie, M. H. Lev, M. S. Rosen, and L. L. Wald, "Two-dimensional imaging in a lightweight portable MRI scanner without gradient coils," *Magnetic Resonance in Medicine*, vol. 73, no. 2, pp. 872–883, Feb. 2015.

[19] C. Z. Cooley, M. W. Haskell, S. F. Cauley, C. Sappo, C. D. Lapierre, C. G. Ha, J. P. Stockmann, and L. L. Wald, "Design of sparse Halbach magnet arrays for portable MRI using a genetic algorithm," *IEEE transactions on magnetics*, vol. 54, no. 1, p. 5100112, Jan. 2018.

[20] Y. Terada, S. Kono, D. Tamada, T. Uchiumi, K. Kose, R. Miyagi, E. Yamabe, and H. Yoshioka, "Skeletal age assessment in children using an open compact MRI system: Skeletal Age Assessment Using Open MRI," *Magnetic Resonance in Medicine*, vol. 69, no. 6, pp. 1697–1702, Jun. 2013. [Online]. Available: https://onlinelibrary.wiley.com/doi/10.1002/mrm.24439

[21] "Skeletal age assessment in children using an open compact MRI system - Terada - 2013 - Magnetic Resonance in Medicine - Wiley Online Library." [Online]. Available: https://onlinelibrary.wiley.com/doi/10.1002/mrm.24439

[22] T. O'Reilly, W. M. Teeuwisse, D. de Gans, K. Koolstra, and A. G. Webb, "In vivo 3D brain and extremity MRI at 50 mT using a permanent magnet Halbach array," *Magnetic Resonance in Medicine*, vol. 85, no. 1, 2021. [Online]. Available: https://onlinelibrary.wiley.com/doi/abs/10.1002/mrm.28396

[23] G. Gold, D. Theodorou, T. Blair, G. Garcia, C. Crowley, F. Rose, D. Trudell, and D. Resnick, "MR Imaging of the Wrist with a Portable Extremity Scanner," p. 1.

[24] S. Ghazinoor and J. V. Crues, "Low Field MRI: A Review of the Literature and Our Experience in Upper Extremity Imaging," *Clinics in Sports Medicine*, vol. 25, no. 3, pp. 591–606, Jul. 2006, publisher: Elsevier. [Online]. Available: https://www.sportsmed.theclinics.com/article/S0278-5919(06)00015-9/fulltext

[25] S. Ghazinoor, J. V. Crues III, and C. Crowley, "Low-field musculoskeletal MRI," *Journal of Magnetic Resonance Imaging*, vol. 25, no. 2, 2007. [Online]. Available: https://onlinelibrary.wiley.com/doi/abs/10.1002/jmri.20854

[26] "Magnevu Mv10000 MRI Scanner - Model Information." [Online]. Available: http://www.dotmed.com/virtual-trade-show/category/MRI/MRI-Scanner/Models/Magnevu/Mv10000/16248

[27] J. V. Crues, F. G. Shellock, S. Dardashti, T. W. James, and O. M. Troum, "Identification of wrist and metacarpophalangeal joint erosions using a portable magnetic resonance imaging system compared to conventional radiographs," *The Journal of Rheumatology*, vol. 31, no. 4, pp. 676–685, Apr. 2004.

[28] D. Price, I. Delakis, C. Renaud, R. Dickinson, and R. Kitney, *Medtronic PoleStar® iMRI Navigation System -portable magnetic resonance imaging system for neurosurgery, Evaluation report*, Oct. 2007.

[29] S. Sluth, "Fair_dealing_guidance_for_students," p. 2.

[30] "Promaxo MRI Technology: Fast, Safe and Accurate | Promaxo," Nov. 2018. [Online]. Available: https://promaxo.com/technology/

[31] "510(k) Premarket Notification." [Online]. Available: https://www.accessdata.fda.gov/scripts/cdrh/cfdocs/cfPMN/pmn.cfm?ID=K202518

[32] G. Sarty, "Personal Communication."

[33] W. A. Grissom, M. Sadinski, A. Nacev, and M. Gomes, "Phase-Based B1 Mapping in a 58-73 mT Single-Sided Prostate MRI Scanner." [Online]. Available: https://www.ismrm.org/workshops/2022/LowField/posters.htm

[34] P. Satya, J. A. Jr, S. S. Venkataraman, D. Kumar, R. Narayanan, A. Nacev, and J. N. M. Jr, "Office-Based, Single-Sided, Low-Field MRI-Guided Prostate Biopsy," *Cureus*, vol. 14, no. 5, May 2022, publisher: Cureus. [Online]. Available: https://www.cureus.com/articles/96127-office-based-single-sided-low-field-mri-guided-prostate-biopsy

[35] Y. Liu, A. T. L. Leong, Y. Zhao, L. Xiao, H. K. F. Mak, A. C. O. Tsang, G. K. K. Lau, G. K. K. Leung, and E. X. Wu, "A low-cost and shielding-free ultra-low-field brain MRI scanner," *Nature Communications*, vol. 12, no. 1, p. 7238, Dec. 2021. [Online]. Available: https://www.nature.com/articles/s41467-021-27317-1

[36] "MR - PET - SPECT - CT - Spectrometers - Clinical - Preclinical - Imaging." [Online]. Available: https://www.mrsolutions.com/

[37] L. L. Tsai, R. W. Mair, M. S. Rosen, S. Patz, and R. L. Walsworth, "An Open-Access, Very-Low-Field MRI System for Posture-Dependent 3He Human Lung Imaging," *Journal of magnetic resonance (San Diego, Calif. : 1997)*, vol. 193, no. 2, pp. 274–285, Aug. 2008. [Online]. Available: https://www.ncbi.nlm.nih.gov/pmc/articles/PMC2572034/

[38] G. Eidmann, R. Savelsberg, P. Blümler, and B. Blümich, "The NMR MOUSE, a Mobile Universal Surface Explorer," *Journal of Magnetic Resonance, Series A*, vol. 122, no. 1, pp. 104–109, Sep. 1996. [Online]. Available: https://www.sciencedirect.com/science/article/pii/S1064185896901850

[39] M. Jones, P. S. Aptaker, J. Cox, B. A. Gardiner, and P. J. McDonald, "A transportable magnetic resonance imaging system for in situ measurements of living trees: The Tree Hugger," *Journal of Magnetic Resonance*, vol. 218, pp. 133–140, May 2012. [Online]. Available: https://www.sciencedirect.com/science/article/pii/S1090780712000766

[40] T. Kimura, Y. Geya, Y. Terada, K. Kose, T. Haishi, H. Gemma, and Y. Sekozawa, "Development of a mobile magnetic resonance imaging system for outdoor tree measurements," *The Review of Scientific Instruments*, vol. 82, no. 5, p. 053704, May 2011.

[41] N. M. Homan, C. W. Windt, F. J. Vergeldt, E. Gerkema, and H. Van As, "0.7 and 3 T MRI and Sap Flow in Intact Trees: Xylem and Phloem in Action," *Applied Magnetic Resonance*, vol. 32, no. 1, pp. 157–170, Aug. 2007. [Online]. Available: https://doi.org/10.1007/s00723-007-0014-3

[42] M. Rokitta, E. Rommel, U. Zimmermann, and A. Haase, "Portable nuclear magnetic resonance imaging system," *Review of Scientific Instruments*, vol. 71, no. 11, pp. 4257–4262, Nov. 2000, publisher: American Institute of Physics. [Online]. Available: https://aip.scitation.org/doi/10.1063/1.1318922

[43] W. Köckenberger, J. M. Pope, Y. Xia, K. R. Jeffrey, E. Komor, and P. T. Callaghan, "A non-invasive measurement of phloem and xylem water flow in castor bean seedlings by nuclear magnetic resonance microimaging," *Planta*, vol. 201, no. 1, pp. 53–63, Mar. 1997. [Online]. Available: https://doi.org/10.1007/BF01258680

[44] H. van As and T. J. Schaafsma, "Noninvasive measurement of plant water flow by nuclear magnetic resonance," *Biophysical Journal*, vol. 45, no. 2, pp. 469–472, Feb. 1984. [Online]. Available: https://www.sciencedirect.com/science/article/pii/S0006349584841703

[45] F. Rabai and R. Ramani, "Chapter 31 - Magnetic Resonance Imaging: Anesthetic Implications," in *Essentials of Neuroanesthesia*, H. Prabhakar, Ed. Academic Press, Jan. 2017, pp. 519–532. [Online]. Available: https://www.sciencedirect.com/science/article/pii/B9780128052990000312

[46] X. Liu, "6.5 NMR Theory and Experiment," Dec. 2021, book Title: Organic Chemistry I Publisher: Kwantlen Polytechnic University. [Online]. Available: https://kpu.pressbooks.pub/organicchemistry/chapter/6-5-the-nmr-theory/

[47] "NMR - Theory," Oct. 2013. [Online]. Available: https://chem.libretexts.org/Bookshelves/Physical_and_Theoretical_Chemistry_Textbook_Maps/Supplemental_Modules_(Physical_and_Theoretical_Chemistry)/Spectroscopy/Magnetic_Resonance_Spectroscopies/Nuclear_Magnetic_Resonance/NMR_-_Theory

[48] F. Bloch, "Nuclear Induction," *Physical Review*, vol. 70, no. 7-8, pp. 460–474, Oct. 1946, publisher: American Physical Society. [Online]. Available: https://link.aps.org/doi/10.1103/PhysRev.70.460

[49] "12.1: Theory of Nuclear Magnetic Resonance (NMR)," Feb. 2016. [Online]. Available: https://chem.libretexts.org/Bookshelves/Organic_Chemistry/Map%3A_Organic_Chemistry_(Wade)/12%3A_Nuclear_Magnetic_Resonance_Spectroscopy/12.01%3A_Theory_of_Nuclear_Magnetic_Resonance

[50] "Magnetic Resonance Imaging (MRI)." [Online]. Available: https://www.nibib.nih.gov/science-education/science-topics/magnetic-resonance-imaging-mri

[51] D. I. Hoult, "Rotating frame zeugmatography," *Journal of Magnetic Resonance (1969)*, vol. 33, no. 1, pp. 183–197, Jan. 1979. [Online]. Available: https://www.sciencedirect.com/science/article/pii/0022236479902026

[52] A. Trakic, J. Jin, E. Weber, and S. Crozier, "Model for B1 Imaging in MRI Using the Rotating RF Field," *Comput. Math. Methods Medicine*, 2014.

[53] R. Kartäusch, T. Driessle, T. Kampf, T. C. Basse-Lüsebrink, U. C. Hoelscher, P. M. Jakob, F. Fidler, and X. Helluy, "Spatial phase encoding exploiting the Bloch-Siegert shift effect," *Magma (New York, N.Y.)*, vol. 27, no. 5, pp. 363–371, Oct. 2014.

[54] E. Torres, T. Froelich, P. Wang, L. DelaBarre, M. Mullen, G. Adriany, D. C. Pizetta, M. J. Martins, E. L. G. Vidoto, A. Tannús, and M. Garwood, "B1 -gradient-based MRI using frequency-modulated Rabi-encoded echoes," *Magnetic Resonance in Medicine*, vol. 87, no. 2, pp. 674–685, Feb. 2022.

[55] S. D. Serai, M.-L. Ho, M. Artunduaga, S. S. Chan, and G. B. Chavhan, "Components of a magnetic resonance imaging system and their relationship to safety and image quality," *Pediatric Radiology*, vol. 51, no. 5, pp. 716–723, May 2021.

[56] D. I. Hoult and R. E. Richards, "The signal-to-noise ratio of the nuclear magnetic resonance experiment," *Journal of Magnetic Resonance (1969)*, vol. 24, no. 1, pp. 71–85, Oct. 1976. [Online]. Available: https://www.sciencedirect.com/science/article/pii/002223647690233X

[57] "Advances in clinical MRI technology." [Online]. Available: https://www.science.org/doi/full/10.1126/scitranslmed.aba2591

[58] M. Parizh, Y. Lvovsky, and M. Sumption, "Conductors for commercial MRI magnets beyond NbTi: requirements and challenges," *Superconductor science & technology*, vol. 30, no. 1, p. 014007, Jan. 2017. [Online]. Available: https://www.ncbi.nlm.nih.gov/pmc/articles/PMC5472374/

[59] T. C. Cosmus and M. Parizh, "Advances in Whole-Body MRI Magnets," *IEEE Transactions on Applied Superconductivity*, vol. 21, no. 3, pp. 2104–2109, Jun. 2011. [Online]. Available: http://ieeexplore.ieee.org/document/5624604/

[60] V. P. Grover, J. M. Tognarelli, M. M. Crossey, I. J. Cox, S. D. Taylor-Robinson, and M. J. McPhail, "Magnetic Resonance Imaging: Principles and Techniques: Lessons for Clinicians," *Journal of Clinical and Experimental Hepatology*, vol. 5, no. 3, pp. 246–255, Sep. 2015. [Online]. Available: https://www.ncbi.nlm.nih.gov/pmc/articles/PMC4632105/

[61] J. C. Sharp and S. B. King, "MRI using radiofrequency magnetic field phase gradients," *Magnetic Resonance in Medicine*, vol. 63, no. 1, 2010. [Online]. Available: https://onlinelibrary.wiley.com/doi/abs/10.1002/mrm.22188

[62] J. C. Sharp, S. B. King, Q. Deng, V. Volotovskyy, and B. Tomanek, "High-resolution MRI encoding using radiofrequency phase gradients: HIGH-RESOLUTION MRI ENCODING USING RADIOFREQUENCY PHASE GRADIENTS," *NMR in Biomedicine*, vol. 26, no. 11, pp. 1602–1607, Nov. 2013. [Online]. Available: https://onlinelibrary.wiley.com/doi/10.1002/nbm.3023

[63] P. Bohidar, H. Sun, G. E. Sarty, and J. C. Sharp, "Trase 1d sequence performance in imperfect b1 fields," *Journal of Magnetic Resonance*, vol. 305, pp. 77–88, 2019. [Online]. Available: https://www.sciencedirect.com/science/article/pii/S1090780719301120

[64] J. C. Sharp and S. B. King, "Mri using radiofrequency magnetic field phase gradients," *Magnetic Resonance in Medicine*, vol. 63, no. 1, pp. 151–161, 2010. [Online]. Available: https://onlinelibrary.wiley.com/doi/abs/10.1002/mrm.22188

[65] A. R. Purchase, T. Pałasz, H. Sun, J. C. Sharp, and B. Tomanek, "A high duty-cycle, multi-channel, power amplifier for high-resolution radiofrequency encoded magnetic resonance imaging," *Magnetic Resonance Materials in Physics, Biology and Medicine*, vol. 32, no. 6, pp. 679–692, Dec. 2019. [Online]. Available: http://link.springer.com/10.1007/s10334-019-00763-1

[66] "B1 transmit phase gradient coil for single-axis TRASE RF encoding - ScienceDirect." [Online]. Available: https://www.sciencedirect.com/science/article/pii/S0730725X13001033?via%3Dihub

[67] "Sarty's USask team tests technology for MRI in space." [Online]. Available: https://news.usask.ca/articles/research/2021/sartys-usask-team-tests-technology-for-mri-in-space.php

[68] "ARTECH HOUSE U.K.: High-Linearity RF Amplifier Design." [Online]. Available: https://uk.artechhouse.com/High-Linearity-RF-Amplifier-Design-P1022.aspx

[69] S. C. Cripps, *RF Power Amplifiers for Wireless Communications, Second Edition*, 2nd ed. Boston: Artech House, May 2006.

[70] "RF Microelectronics: Razavi, Behzad: 9780137134731: Books - Amazon.ca." [Online]. Available: https://www.amazon.ca/RF-Microelectronics-2nd-Behzad-Razavi/dp/0137134738

[71] F. Raab, P. Asbeck, S. Cripps, P. Kenington, Z. Popovic, N. Pothecary, J. Sevic, and N. Sokal, "Power amplifiers and transmitters for RF and microwave," *IEEE Transactions on Microwave Theory and Techniques*, vol. 50, no. 3, pp. 814–826, Mar. 2002. [Online]. Available: http://ieeexplore.ieee.org/document/989965/

[72] T. H. Lee, *The Design of CMOS Radio-Frequency Integrated Circuits*, 2nd ed. Cambridge, UK ; New York: Cambridge University Press, Dec. 2003.

[73] F. Raab, P. Asbeck, S. Cripps, P. Kenington, Z. Popović, N. Pothecary, J. Sevic, and N. Sokal, "Power amplifiers and transmitters for RF and microwave," 2002.

[74] P. B. Kenington, *High Linearity RF Amplifier Design*. Boston, MA: Artech House Publishers, Sep. 2000.

[75] W. Storr, "Amplifier Classes and the Classification of Amplifiers," Jul. 2013. [Online]. Available: https://www.electronics-tutorials.ws/amplifier/amplifier-classes.html

[76] M. Twieg and M. A. Griswold, "High efficiency radiofrequency power amplifier module for parallel transmit arrays at 3 Tesla," *Magnetic Resonance in Medicine*, vol. 78, no. 4, 2017. [Online]. Available: https://onlinelibrary.wiley.com/doi/abs/10.1002/mrm.26510

[77] B. N. Reid, V. Christopher, G. William A., and G. Mark A., "Low-cost Modular RFPA Platform for Gradient-Free Quantitative Imaging." [Online]. Available: https://www.ismrm.org/workshops/2022/LowField/breakout.htm

[78] "(ISMRM 2020) MR Barcoding: Gradient-Free MRI Using B1-Selective Parallel Transmission." [Online]. Available: https://archive.ismrm.org/2020/0620.html

[79] J. T. Vaughan and D. Myer, "RF Coil Element Mounted Power Amplifiers," p. 1.

[80] H. J, R. MJ, O. H, and G. MA, "High power, high efficiency on-coil current-mode amplifier for parallel transmission arrays," *In Proceedings of the 15th Annual Meeting of ISMRM*, 2007. [Online]. Available: https://www.semanticscholar.org/paper/High-power%2C-high-efficiency-on-coil-current-mode-Heilman-Riffe/0a8e5bedbed0b91a1d82752edb9b39a5282840b2

[81] "Amateur Radio Station W6PQL." [Online]. Available: https://www.w6pql.com/

[82] "6-2017 RF deck." [Online]. Available: https://www.w6pql.com/hf/62017_rf_deck.htm

[83] "1 KW SSPA for 1.8-54 MHz." [Online]. Available: https://www.w6pql.com/1_kw_sspa_for_1_8-54_mhz.htm